NASA Contractor Report 166152

(P Georgian)

An Alternating-Direction-Implicit Algorithm for the Unsteady Potential Equation in Conservation Form

Richard R. Chipman

July 1980

NASA
National Aeronautics and Space Administration

AN ALTERNATING-DIRECTION-IMPLICIT ALGORITHM FOR THE UNSTEADY POTENTIAL EQUATION IN CONSERVATION FORM

By Richard R. Chipman

July 1980

Prepared under Contract No. NAS2-10487
by
Grumman Aerospace Corporation
Bethpage, N.Y. 11714

for

AMES RESEARCH CENTER

NATIONAL AERONAUTICS AND SPACE ADMINISTRATION

ACKNOWLEDGMENTS

Funding for this work was provided jointly by the Applied Computational Aerodynamics Branch of NASA Ames and the Structural Mechanics Division of AFWAL. Dr. Peter Goorjian of Ames was the contract technical monitor.

A pilot code based on the untransformed flow equations (non-airfoil-adapted grid) was developed under a subcontract with Dr. Antony Jameson. He also provided significant technical consultation in various aspects of the project.

Mr. Edward Laurie of Grumman Aerospace Corporation assisted in running comparison calculations and in generating the computer-graphics display of results.

CONTENTS

ILLUSTRATIONS

AN ALTERNATING-DIRECTION-IMPLICIT ALGORITHM FOR THE UNSTEADY POTENTIAL EQUATION IN CONSERVATION FORM

Richard R. Chipman
Grumman Aerospace Corporation

1 - SUMMARY

An implicit finite-difference scheme is presented for the efficient computation of unsteady potential flow about airfoils. The formulation uses density and velocity potential as dependent variables, and is cast in conservation form to assure the theoretically correct determination of shockwave location and speed. To enable boundary conditions to be imposed directly on the airfoil surface, a time-varying sheared-rectilinear coordinate transformation is employed. Calculated time-history solutions on a pulsating airfoil are compared with the results of another unsteady transonic code. The method is demonstrated to have excellent numerical stability and to give accurate solutions with sharply resolved shocks.

2 - INTRODUCTION

The transonic flow regime has long been known to be the most critical for flutter and other unsteady aeroelastic phenomena. Until recently, there was no efficient method for calculating unsteady aerodynamics in this speed range; consequently, transonic flutter prediction has relied on wind tunnel testing. With the advent of faster computers and the emphasis on transonic cruise and maneuver capabilities for new aircraft design, much progress has been recently made in the development of both steady and unsteady transonic computational methods.

In unsteady transonic aerodynamics, work has proceeded along two distinct lines. In the first, researchers have produced linearized unsteady solutions about nonlinear mean (steady) flows. The efforts of Ehlers[1]; Traci, Albano, and Farr[2]; Cunningham[3]; Liu[4]; and Fung, Yu, and Seebass[5] are examples of this approach. From experimental measurements, such as those

of Tijdeman[6], it has been obvious that these linearized solutions are only valid for a limited set of problems. Consequently, other researchers have pursued a second approach - the use of finite-difference methods to obtain solutions to the coupled steady/unsteady flow. In this area, the works of Magnus and Yoshihara[7]; Lerat and Sides[8]; Beam and Warming[9]; Ballhaus and Steger[10]; Ballhaus and Goorjian[11-12]; Isogai[13]; Chipman and Jameson[14]; Goorjian[15]; and Sankar and Tassa[16] are notable. The first three cited efforts in coupled steady/unsteady flow have produced methods for solving the full Euler equations, which (although computationally too expensive for routine use) do provide excellent benchmark calculations. Ballhaus' works have produced an efficient method for solving the low-frequency, small-perturbation form of the potential equation, thus making possible economic solutions to a range of important transonic unsteady problems.

To extend this range, the latter four works have solved the full-potential flow equations. Isogai developed the first such procedure. The next two works are improvements in that: (1) conservation-law form is used to accurately locate shock waves in space and time; and (2) the ADI scheme is used for computational efficiency. The Chipman-Jameson method uses density and velocity components as dependent variables, giving a simple system of first-order equations to be solved. The Goorjian method uses velocity potential as the dependent variable and, by time-linearizing the density, derives a single (though complicated) scalar equation. The method of Sankar and Tassa uses the strongly-implicit-procedure algorithm and has been formulated both in conservative and nonconservative form; thus far, the scheme has been coded only in nonconservative form.

The present method uses both the density and velocity potential as dependent variables, resulting in a simple system of two equations. It is a significant improvement over the authors' previous method[14] in that the use of the potential function totally eliminates numerically created vorticity present in the prior method. Furthermore, it retains the desirable features of conservation form and efficient implicit differencing.

The theoretical development of the present method is given in Section 4 of this report. The discussion covers the basic flow equation, the details of the

alternating-direction-implicit (ADI) algorithm, the addition of artificial-viscosity terms to capture shocks, the introduction of a time-varying sheared-rectilinear coordinate transformation, the specification of the boundary conditions, and the implementation of the method for a specific test problem - an airfoil pulsating in thickness.

In Section 5, the test problem is discussed in detail, and computed results are presented. These results are compared with those of Reference 15. Also studies of the effect of variations in the time-step size and artificial viscosity are summarized.

Section 6 presents conclusions and recommendations.

3 - LIST OF SYMBOLS

a	= local speed of sound
$D_x(\ )$	= central difference in x of enclosed quantity
$D_y(\ )$	= central difference in y of enclosed quantity
$\{f(T,\{W\})\}$	= vector function of T and the vector W
h	= stagnation enthalpy
J	= Jacobian of transformation
M	= Mach number
$(\ )^n$	= n-th time level of enclosed quantity
r1, r2	= right-hand side of Eq (9) or Eq (26)
S(x,t)	= instantaneous airfoil-surface location
t, T	= time
u, U	= streamwise component of velocity, ξ-aligned contravariant velocity component
v, V	= stream-normal component of velocity, η-aligned contravariant velocity component
$\{W\}$	= general vector (in this case, having components ρ and ϕ)
x,y	= untransformed coordinates
z(x,y,t)	= surface of flow discontinuity
γ	= specific heat ratio

$\Delta(\ )$ = time increment of enclosed quantity

ε = artificial viscosity coefficient

ξ, η = transformed coordinates

μ = see Eq (6)

ρ = density

ϕ = velocity potential

$(\ )_m$ = partial derivative of enclosed quantity with respect to "m" variable

$(\ )_\infty$ = free-stream value of enclosed quantity

$\Delta(\hat{\ })$ = solution to Eq (11)

4 - THEORY

Basic Flow Equations

For unsteady, two-dimensional, isentropic potential flow, the equations of conservation of mass and momentum can be written

$$\rho_t + (\rho\phi_x)_x + (\rho\phi_y)_y = 0 \tag{1}$$

$$\phi_t + h = 0, \tag{2}$$

where

$$h = \tfrac{1}{2}(\phi_x^2 + \phi_y^2) + \frac{\rho^{\gamma-1}}{(\gamma - 1)M_\infty^2} - h_\infty. \tag{3}$$

(Equation (2) is called the integrated unsteady Bernoulli equation.) Both equations are in conservation form, albeit (2) is considered weak-conservation form. Hence, (1) conserves mass across shocks, where the flow variables are discontinuous, and results in the jump condition

$$[\rho]\, z_t + [\rho u]\, z_x + [\rho v]\, z_y = 0, \tag{4}$$

where $z(x,y,t) = 0$ represents the surface of discontinuity and [ ] denotes the jump of the enclosed variables across the discontinuity.

Implicit Algorithm

To simplify the ensuing discussion, (1) and (2) are represented by the vector equation

$$\{W\}_t + \{f(t,\{W\})\} = 0. \tag{5}$$

A family of difference schemes for solving this system is

$$\{\Delta W\} + \mu \Delta t \{f^{n+1}\} + (1-\mu)\Delta t\{f^n\} = 0, \tag{6}$$

$$0 \le \mu \le 1,$$

where n and n + 1 denote the present and new time levels. For $\mu = 0$, the scheme is explicit; otherwise it is implicit. The case $\mu = 1/2$ is the standard Crank-Nicolson scheme,[17] which has second-order accuracy. Using a Taylor series expansion, the variables at the new time can be written

$$\{f^{n+1}\} = \{f^n\} + \frac{\partial}{\partial t}\{f^n\}\Delta t + O(\Delta t^2).$$

$$= \{f^n\} + \nabla \cdot \{\Delta W\}\{f^n\} + O(\Delta t^2). \tag{7}$$

Substitution into (6) gives

$$\{\Delta W\} + \mu \Delta t(\nabla \cdot \{\Delta W\})\{f^n\} = -\Delta t\{f^n\} - O(\Delta t^2) \tag{8}$$

where all coefficients appear at time n.

This scheme is now rewritten in the original variables of (1) and (2), and centered differences are used to evaluate the divergence terms. Thus, the following system of equations is obtained for each interior point of the computational grid:

$$\begin{bmatrix} 1+\mu\Delta t(D_x u + D_y v) & \mu\Delta t(D_x \rho D_x + D_y \rho D_y) \\ \mu\Delta t\left(\frac{a^2}{\rho}\right) & 1+\mu\Delta t(uD_x + vD_y) \end{bmatrix} \begin{Bmatrix} \Delta\rho \\ \Delta\phi \end{Bmatrix} = \begin{Bmatrix} r1 \\ r2 \end{Bmatrix}, \tag{9}$$

where

$$\begin{Bmatrix} r1 \\ r2 \end{Bmatrix} = -\Delta t \begin{Bmatrix} D_x \rho u + D_y \rho v \\ h \end{Bmatrix},$$

$$u = \phi_x, \quad v = \phi_y,$$

$$\Delta(\ ) = (\ )^{n+1} - (\ )^n.$$

Approximate Factorization

The matrix on the left-hand side of (9) can be approximately factored as

$$\begin{bmatrix} 1+\mu\Delta t\, D_y v & \mu\Delta t\, D_y \rho D_y \\ \mu\Delta t\left(\frac{a^2}{\rho}\right) & 1+\mu\Delta t\, v D_y \end{bmatrix} \cdot \begin{bmatrix} 1+\mu\Delta t\, D_x u & \mu\Delta t\, D_x \rho D_x \\ 0 & 1+\mu\Delta t\, u D_x \end{bmatrix} \tag{10}$$

However, this scheme is not unconditionally stable. A small modification of (10), which introduces error of order ΔT^3, does result in an unconditionally stable scheme. This modification consists of replacing the lower right-hand term of the second matrix by

$$1+\mu\Delta t\, u D_x - \mu^2\Delta t^2 (a^2/\rho)\, D_x \rho D_x .$$

The resulting alternating sweeps of this stable scheme are

- x-sweep:

$$\begin{bmatrix} 1+\mu\Delta t\, D_y v & \mu\Delta t\, D_y \rho D_y \\ \mu\Delta t\left(\frac{a^2}{\rho}\right) & 1+\mu\Delta t\, v D_y \end{bmatrix} \begin{Bmatrix} \Delta\hat{\rho} \\ \Delta\hat{\phi} \end{Bmatrix} = \begin{Bmatrix} r1 \\ r2 \end{Bmatrix} \tag{11}$$

- y-sweep:

$$\begin{bmatrix} 1+\mu\Delta t\, D_x u & \mu\Delta t\, D_x \rho D_x \\ 0 & 1+\mu\Delta t\, u D_x - (\mu^2\Delta t^2 a^2/\rho) D_x \rho D_x \end{bmatrix} \begin{Bmatrix} \Delta\rho \\ \Delta\phi \end{Bmatrix} = \begin{Bmatrix} \Delta\hat{\rho} \\ \Delta\hat{\phi} \end{Bmatrix} . \tag{12}$$

Artificial Viscosity

To capture shocks, artificial-viscosity terms of the Jameson type[18] are added to the upper-left portions of each equation and to r1. Respectively, these terms are

$$\begin{aligned} &-\epsilon\,\Delta t \Delta y D_y^2 \\ &-\epsilon\,\Delta t \Delta x D_x^2 \\ &\epsilon\,\Delta t (\Delta x D_x^2 \rho + \Delta y D_y^2 \rho), \end{aligned} \tag{13}$$

where ϵ is a constant, typically equal to 0.15.

Alternate schemes for incorporating artificial viscosity in a more selective manner are possible. One such alternative is to switch the coefficient ϵ from a low value in regions where the flow is subsonic to a higher value in supersonic regions; i.e.,

$$\epsilon = \epsilon_0 + \epsilon_1 \cdot \max\left(0., \; 1 - \left(\frac{M_c}{M}\right)^2\right), \tag{14}$$

where ϵ_0 = artificial viscosity in "subsonic" zones ($M \leq M_c$)

ϵ_1 = maximum amount of artificial viscosity added to "supersonic" zones ($M > M_c$)

M = local Mach number

M_c = cutoff Mach number (typically 0.95).

Another scheme is to vary the viscosity based on gradients in the flow field; e.g.,

$$\epsilon = \epsilon_0 + \epsilon_1 \cdot \left(\frac{\phi_{i+1,j} - 2\phi_{i,j} + \phi_{i-1,j}}{|\phi_{i+1,j}| + 2|\phi_{i,j}| + |\phi_{i-1,j}|}\right) . \tag{15}$$

When such schemes are used, however, care must be taken to retain conservation form in the basic equations. Thus, for example, the first term of Expressions (13) must be replaced by

$$-\Delta t \Delta y D_y(\epsilon D_y). \tag{16}$$

In the present work, only the constant (non-switched) form of artificial viscosity has been used. Future efforts could easily include the switching concept.

Airfoil-Adapted Coordinate Transformation

To conveniently impose the airfoil boundary conditions, a time-varying coordinate transformation can be introduced to (1) and (2). The general form of such a transformation is

$$\xi = \xi(x,y,t), \quad \eta = \eta(x,y,t), \quad T = t \; . \tag{17}$$

Equations (1) and (2) transform as

$$\rho_T + \left(\frac{\rho U}{|J|}\right)_\xi + \left(\frac{\rho V}{|J|}\right)_\eta = 0,$$

$$\phi_T + h = 0, \tag{18}$$

where J is the Jacobian of the transformation and U and V are the contravariant velocity components, given by

$$U = \xi_t + \xi_x u + \xi_y v$$

$$V = \eta_t + \eta_x u + \eta_y v \tag{19}$$

To preserve a factorable form of the equations, cross terms arising when (19) is introduced into (18) are explicitly differenced. This technique is illustrated below.

For the particular sample problem used in this study (see subsection, Sample Problem), a simple time-varying sheared-rectilinear coordinate transformation is used

$$\xi = x, \quad \eta = y - S(x,t), \quad T = t, \tag{20}$$

where S is the instantaneous airfoil surface location as noted in Fig. 1. For this case, the determinant of J is 1 and (19) become

$$U = \phi_\xi - S_\xi \phi_\eta$$

$$V = -\phi_\xi S_\xi + \phi_\eta (1 + S_\xi^2) - S_T . \tag{21}$$

Substitution into (18) gives

$$\rho_T + (\rho\phi_\xi)_\xi + (\rho[-S_T + (1+S_\xi^2)\,\phi_\eta])_\eta = (\rho S_\xi \phi_\eta)_\xi + (\rho S_\xi \phi_\xi)_\eta$$

$$\phi_T + \frac{\rho^{\gamma-1}}{(\gamma-1)M_\infty^2} + \tfrac{1}{2}[\phi_\xi^2 + (1+S_\xi^2)\,\phi_\eta^2] - h_\infty = S_\xi \phi_\xi \phi_\eta \tag{22}$$

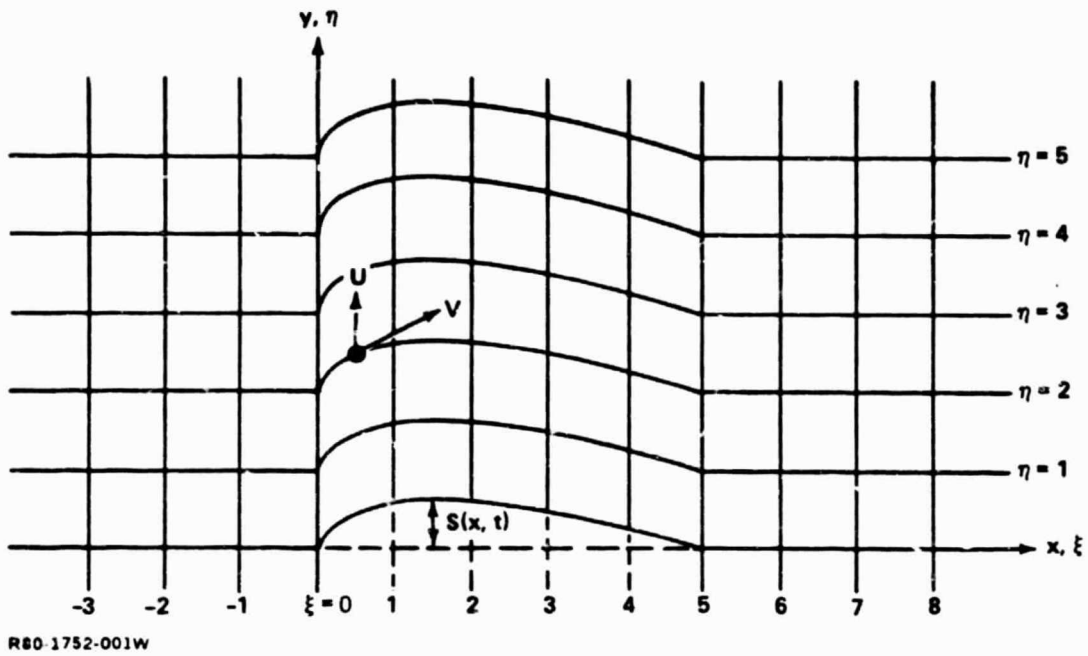

Figure 1. — Shearing Transformation

The implicit algorithm developed previously is now applied to this system; however the cross terms, grouped on the right-hand side of (22), are handled explicitly. The resulting equations are

$$\Delta\rho + \mu\Delta T\left(\frac{\partial}{\partial\xi}\,\bar{u} + \frac{\partial}{\partial\eta}\,[-S_T + \bar{v}]\right)\Delta\rho + \mu\Delta T\left(\frac{\partial}{\partial\xi}\,\rho\,\frac{\partial}{\partial\xi} + \frac{\partial}{\partial\eta}\,\bar{\rho}\,\frac{\partial}{\partial\eta}\right)\Delta\phi$$

$$+\Delta T\left(\frac{\partial}{\partial\xi}\,\rho U + \frac{\partial}{\partial\eta}\,\rho V\right) = 0,$$

$$\Delta\phi + \mu\Delta T(a^2/\rho)\,\Delta\rho + \mu\Delta T\left(\bar{u}\,\frac{\partial}{\partial\xi} + \bar{v}\,\frac{\partial}{\partial\eta}\right)\Delta\phi \quad + \Delta T\,h = 0, \tag{23}$$

where "a" is the local speed of sound and

$$\bar{u} = \phi_\xi, \quad \bar{v} = (1 + S_\xi^2)\,\phi_\eta, \quad \bar{\rho} = (1 + S_\xi^2)\,\rho. \tag{24}$$

Replacing the indicated partial derivatives by central-difference operators, D, one obtains the following matrix equation:

$$\begin{bmatrix} 1+\mu\Delta T(D_\xi \Pi + D_\eta(\nabla - S_T)) & \mu\Delta T(D_\xi \rho D_\xi + D_\eta \bar{\rho} D_\eta) \\ \mu\Delta T\left(\frac{a^2}{\rho}\right) & 1+\mu\Delta T(\Pi D_\xi + \nabla D_\eta) \end{bmatrix} \begin{Bmatrix} \Delta\rho \\ \Delta\phi \end{Bmatrix} = -\Delta T \begin{Bmatrix} D_\xi \rho U + D_\eta \rho V \\ h \end{Bmatrix}. \quad (25)$$

Following the factorization procedure previously outlined and introducing the artificial viscosity terms, one obtains the final difference equations:

- ξ - sweep

$$\begin{bmatrix} 1+\mu\Delta T D_\eta(\nabla - S_T) - \epsilon\Delta T\Delta\eta D_\eta^2 & \mu\Delta T D_\eta \bar{\rho} D_\eta \\ \mu\Delta T\left(\frac{a^2}{\rho}\right) & 1+\mu\Delta T\nabla D_\eta \end{bmatrix} \begin{Bmatrix} \Delta\hat{\rho} \\ \Delta\hat{\phi} \end{Bmatrix} = -\Delta\dot{T} \begin{Bmatrix} r1 \\ r2 \end{Bmatrix}, \quad (26)$$

where

$$\begin{Bmatrix} r1 \\ r2 \end{Bmatrix} = \begin{Bmatrix} D_\xi \rho U + D_\eta \rho V - \epsilon(\Delta\xi D_\xi^2 + \Delta\eta D_\eta^2)\rho \\ h \end{Bmatrix}.$$

- η - sweep

$$\begin{bmatrix} 1+\mu\Delta T D_\xi \Pi - \epsilon\Delta T\Delta\xi D_\xi^2 & \mu\Delta T D_\xi \rho D_\xi \\ 0 & 1+\mu\Delta T\Pi D_\xi - \left(\frac{\mu^2\Delta T^2 R^2}{\rho}\right) D_\xi \rho D_\xi \end{bmatrix} \begin{Bmatrix} \Delta\rho \\ \Delta\phi \end{Bmatrix} = \begin{Bmatrix} \Delta\hat{\rho} \\ \Delta\hat{\phi} \end{Bmatrix} \quad (27)$$

Discretization

In (26) and (27), differences will be centered about (i,j) and will span 2 mesh widths (3 points); consequently, the operators $(D_\eta \rho D_\eta)$ and $(D_\xi \rho D_\xi)$ will spread to 4 mesh widths (5 points). The equation for the j-th mesh point in (26) may then be written in the form

$$[A]\{\Delta\hat{W}\}_{j-2}+[B]\{\Delta\hat{W}\}_{j-1}+[C]\{\Delta\hat{W}\}_{j}+[D]\{\Delta\hat{W}\}_{j+1}+[E]\{\Delta\hat{W}\}_{j+2}=\{r\} \tag{28}$$

where the coefficients of $\{\Delta W\}$ for mesh points outside the range j - 2 to j + 2 are zero. If (26) is multiplied by $2(\Delta\eta)_j/\Delta T$, the coefficients in (28) become

$$[A]=\begin{bmatrix} 0 & (\bar{\rho}/2\Delta\eta)_{j-1} \\ 0 & 0 \end{bmatrix}, \quad [E]=\begin{bmatrix} 0 & (\bar{\rho}/2\Delta\eta)_{j+1} \\ 0 & 0 \end{bmatrix}$$

$$[B]=\begin{bmatrix} (\nabla-S_T)_{j-1} & 0 \\ 0 & \nabla_j \end{bmatrix}, \quad [D]=\begin{bmatrix} (-\nabla+S_T)_{j+1} & 0 \\ 0 & -\nabla_j \end{bmatrix}$$

$$[C]=\begin{bmatrix} \frac{2}{\mu\Delta T}\Delta\eta_j+\frac{4\epsilon}{\mu} & -\left(\frac{\bar{\rho}}{2\Delta\eta}\right)_{j-1}-\left(\frac{\bar{\rho}}{2\Delta\eta}\right)_{j+1} \\ 2\left(\frac{\Delta\eta a^2}{\rho}\right)_j & \frac{2}{\mu\Delta T}\Delta\eta_j \end{bmatrix} \tag{29}$$

A similar set of matrices can be obtained from (27).

Stretchings

For computational efficiency, simple grid stretchings also are introduced:

$$\bar{\xi}=\bar{\xi}(\xi) \quad \text{and} \quad \bar{\eta}=\bar{\eta}(\eta). \tag{30}$$

The effect of these transformations on the equations to be solved is simply to introduce the derivatives of the stretching functions as multipliers of the terms containing spatial derivatives. The details of the particular stretchings used are discussed in the Sample Problem subsection.

Solution Procedure

If equations similar to (28) are written for all mesh points and combined into one system of equations corresponding to (26), the result is a system of

block-five-diagonal matrix equations. This can be solved efficiently by a splitting procedure. Thus, (26) is rewritten as

$$[M]\{\Delta\hat{W}\} = \{r\}, \tag{31}$$

where

$$[M] = \begin{bmatrix} C_1 & D_1 & E_1 & 0 & 0 & 0 & 0 & \cdot & \cdot \\ B_2 & C_2 & D_2 & E_2 & 0 & 0 & 0 & \cdot & \cdot \\ A_3 & B_3 & C_3 & D_3 & E_3 & 0 & 0 & \cdot & \cdot \\ 0 & A_4 & B_4 & C_4 & D_4 & E_4 & 0 & \cdot & \cdot \\ \cdot & \cdot & \cdot & \cdot & \cdot & \cdot & \cdot & \cdot & \cdot \\ \cdot & \cdot & \cdot & \cdot & \cdot & \cdot & \cdot & \cdot & \cdot \end{bmatrix},$$

or in split form as

$$[L]\cdot[U]\{\Delta\hat{W}\} = \{r\},$$

where

$$[L] = \begin{bmatrix} \gamma_1 & 0 & 0 & 0 & \cdot & \cdot \\ \beta_2 & \gamma_2 & 0 & 0 & \cdot & \cdot \\ \alpha_3 & \beta_3 & \gamma_3 & 0 & \cdot & \cdot \\ 0 & \alpha_4 & \beta_4 & \gamma_4 & \cdot & \cdot \\ \cdot & \cdot & \cdot & \cdot & \cdot & \cdot \\ \cdot & \cdot & \cdot & \cdot & \cdot & \cdot \end{bmatrix}, \quad [U] = \begin{bmatrix} 1 & -\delta_1 & -\epsilon_1 & 0 & 0 & \cdot & \cdot \\ 0 & 1 & -\delta_2 & -\epsilon_2 & 0 & \cdot & \cdot \\ 0 & 0 & 1 & -\delta_3 & -\epsilon_3 & \cdot & \cdot \\ 0 & 0 & 0 & 1 & -\delta_4 & \cdot & \cdot \\ \cdot & \cdot & \cdot & \cdot & \cdot & \cdot & \cdot \\ \cdot & \cdot & \cdot & \cdot & \cdot & \cdot & \cdot \end{bmatrix}$$

Expanding the product LU and comparing with M, one obtains the following relationships between the elements of M, L, and U:

$$\begin{aligned} \alpha_j &= A_j, & \delta_j &= -[\gamma_j]^{-1}(D_j + \beta_j\epsilon_{j-1}), \\ \beta_j &= B_j + \alpha_j\delta_{j-2}, & \epsilon &= -[\gamma_j]^{-1}E_j. \\ \gamma_j &= C_j + \alpha_j\epsilon_{j-2} + \beta_j\delta_{j-1}, \end{aligned} \tag{32}$$

Then, the solution is obtained by sequentially solving

$$[L]\{z\} = \{r\}$$
$$[U]\{\Delta\hat{W}\} = \{z\}. \tag{33}$$

Thus,

$$z_j = [\gamma_j]^{-1}(r_j - \alpha_j z_{j-2} - \beta_j z_{j-1}),$$
$$\Delta\hat{W}_j = z_j + \delta_j(\Delta\hat{W}_{j+1}) + \epsilon_j(\Delta\hat{W}_{j+2}), \tag{34}$$

where the first solution is obtained by a forward sweep in j and the second by a reverse sweep. An identical procedure is used to obtain a solution for (27).

To initialize and terminate the sweeps, the difference equations are modified to incorporate the presence of the boundaries. At the lower boundary, for example, we choose to backward difference the ρ- and v-type terms (so that no physical variables are defined outside the computational space) and to retain central differences in ϕ terms by introducing a row of dummy points just below $\eta = 0$. Before and after the sweeps are completed, the boundary conditions (discussed below) are enforced.

Boundary Conditions

On the airfoil surface, tangential flow is maintained. In the transformed coordinates, this is equivalent to

$$V = 0, \quad \text{for } \eta = 0 \quad \text{and} \quad \xi_{LE} \le \xi \le \xi_{TE}, \tag{35}$$

where subscripts LE and TE denote the airfoil leading and trailing edges, respectively. For the nonlifting symmetric-airfoil problem studied, the flow is symmetric about $\eta = 0$; consequently, only half the flow field is modeled. Thus,

$$\phi_\eta = 0, \quad \text{for } \eta = 0 \quad \text{and} \quad \xi \le \xi_{LE} \text{ or } \xi \ge \xi_{TE}. \tag{36}$$

The uniform onset flow in the far field is assumed to be undisturbed; i.e., acoustic waves originating at the airfoil do not have sufficient time to reach the outer boundaries. Thus,

$$(u, v) = (1, 0),$$

or

$$v = \phi_\eta = 0,$$

$$u = \phi_\xi - S_\xi \phi_\eta = \phi_\xi = 1.$$

Hence,

$$(\phi_\xi, \phi_\eta) = (1, 0), \quad \text{for } \eta = \eta_{max} \text{ and } \xi = \pm \xi_{max}, \tag{37}$$

where the subscripts "max" denote the far-field boundaries of the computational mesh. In Fig. 2, the boundary conditions are marked on a sketch of the computational space.

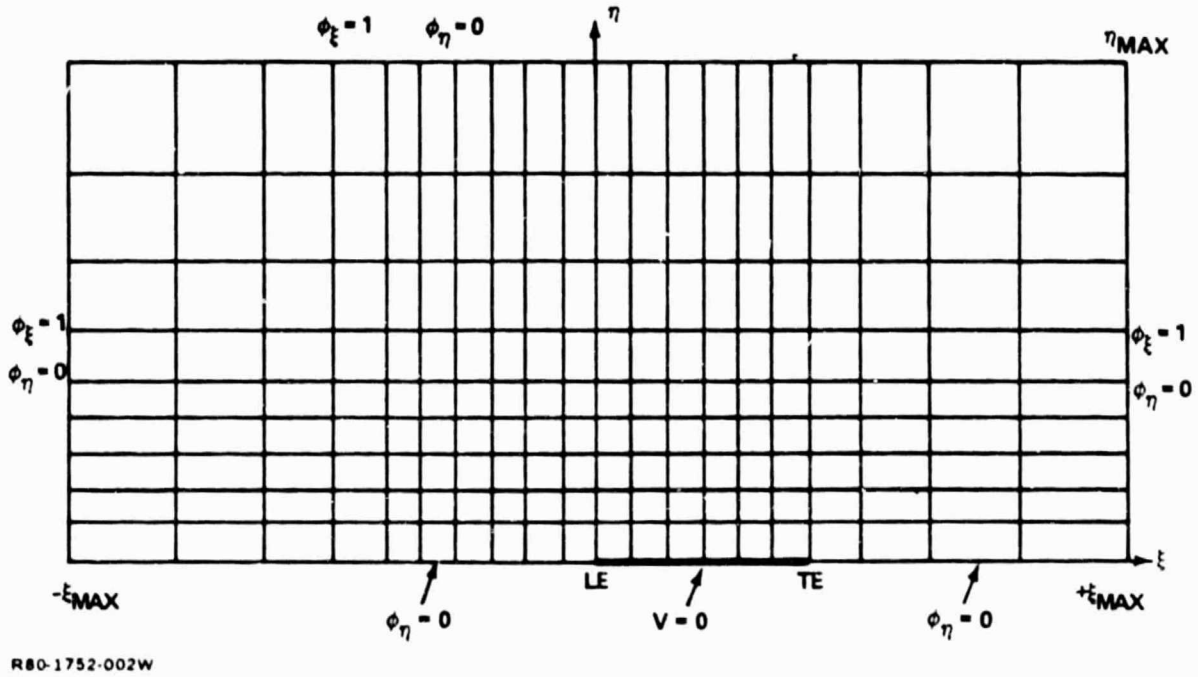

Figure 2. – Boundary Conditions in the Computational Grid.

Implementation
(Codes UFLO3 and UFLO4)

The algorithm was coded for the pulsating-airfoil sample problem to be described below. A version (UFLO3) using the original untransformed equations was written, as well as a version (UFLO4) employing the time-varying coordinates. For UFLO3, the airfoil boundary conditions were applied on the slit, y = 0 (mean chordline); whereas, in UFLO4, they were applied on the η = 0 line coincident with the instantaneous airfoil surface position.

5 - RESULTS

Sample Problem

A problem that has been analyzed by several researchers is that of computing unsteady pressures on a parabolic-arc airfoil which successively thickens and thins during its travel, as shown in Fig. 3. The Mach number for this example is 0.85. The equations governing the variation of thickness are

$$TH = \frac{1}{10}\left[10 - 15\left(\frac{T}{15}\right) + 6\left(\frac{T}{15}\right)^2\right]\cdot\left(\frac{T}{15}\right)^3, \quad 0 \le T \le 15,$$

$$TH = \frac{1}{10}\left[10 - 15\left(\frac{30-T}{15}\right) + 6\left(\frac{30-T}{15}\right)^2\right]\cdot\left(\frac{30-T}{15}\right)^3, \quad 15 \le T \le 30,$$

$$TH = 0, \quad 30 \le T, \tag{38}$$

where TH is the midcord thickness ratio and T is time, measured in chordlengths traveled. Consequently, the airfoil initially has zero thickness, grows to its maximum thickness of 10% after traveling 15 chordlengths and returns to

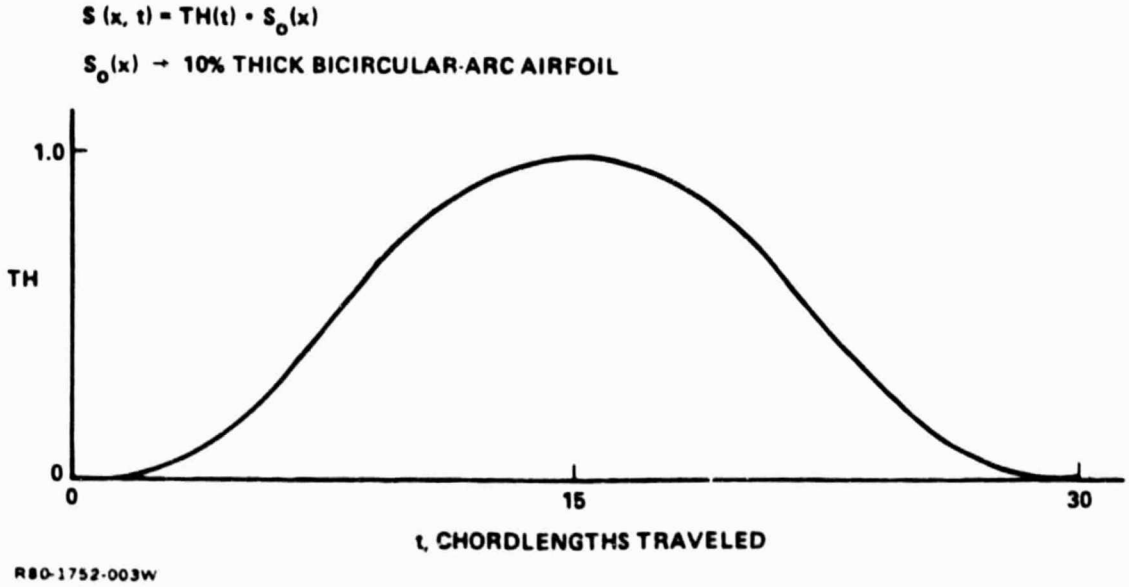

Figure 3. — Pulsating Parabolic-Arc Airfoil.

zero thickness after traveling a total of 30 chordlengths. During the course of this travel, the variation of thickness causes an interesting flow-structure. A strong shock wave forms on the airfoil as it thickens; subsequently, as the airfoil thins, the shock propagates rapidly upstream and leaves the airfoil nose to enter the oncoming flow. The numerical computation of this extensive shock motion is a rigorous test for unsteady transonic aerodynamic codes. It might be noted that, because of their basic theoretical limitations, the methods of Ref. 1-5 are unable to handle such cases of large shock motion.

The computational grid used consists of 152 points in the streamwise direction and 40 in the stream-normal direction. To facilitate comparisons, the grid is patterned after that of Ref. 15. In the streamwise direction, the grid is uniform over the interval that extends from one chordlength upstream of the airfoil nose to the trailing edge; to either side of this interval, the grid is smoothly stretched to the boundaries located more than 30 chordlengths from the airfoil. In the stream-normal direction, the grid is uniform from the airfoil surface to a distance of 0.2 chordlengths; beyond this point, the grid is stretched smoothly to a boundary also more than 30 chordlengths from the airfoil. The minimum grid spacing is roughly 0.02 chordlengths in each direction. From studies of grid variation, it was concluded that the solution is sensitive to the choice of grids but that the present choice is adequate because it combines a fine-grid structure near the airfoil with boundaries sufficiently far removed for the present calculations. Appendix A presents the actual mesh used.

Unless otherwise noted, all calculations using either UFLO3 or UFLO4 were performed with a time step of $\Delta T = 0.02$ chordlengths traveled and an artifical viscosity coefficient of $\epsilon = 0.15$. Runs varying these parameters are described in separate subsections below.

UFLO3 and UFLO4 Results

Using UFLO3, a time history of the flow about the pulsating airfoil was calculated. The resulting pressure coefficient distributions for six time slices are shown in Fig. 4. At the first time slice, the flow is subcritical. During the next two, a shock forms, strengthens, and moves aft. A slight re-expan-

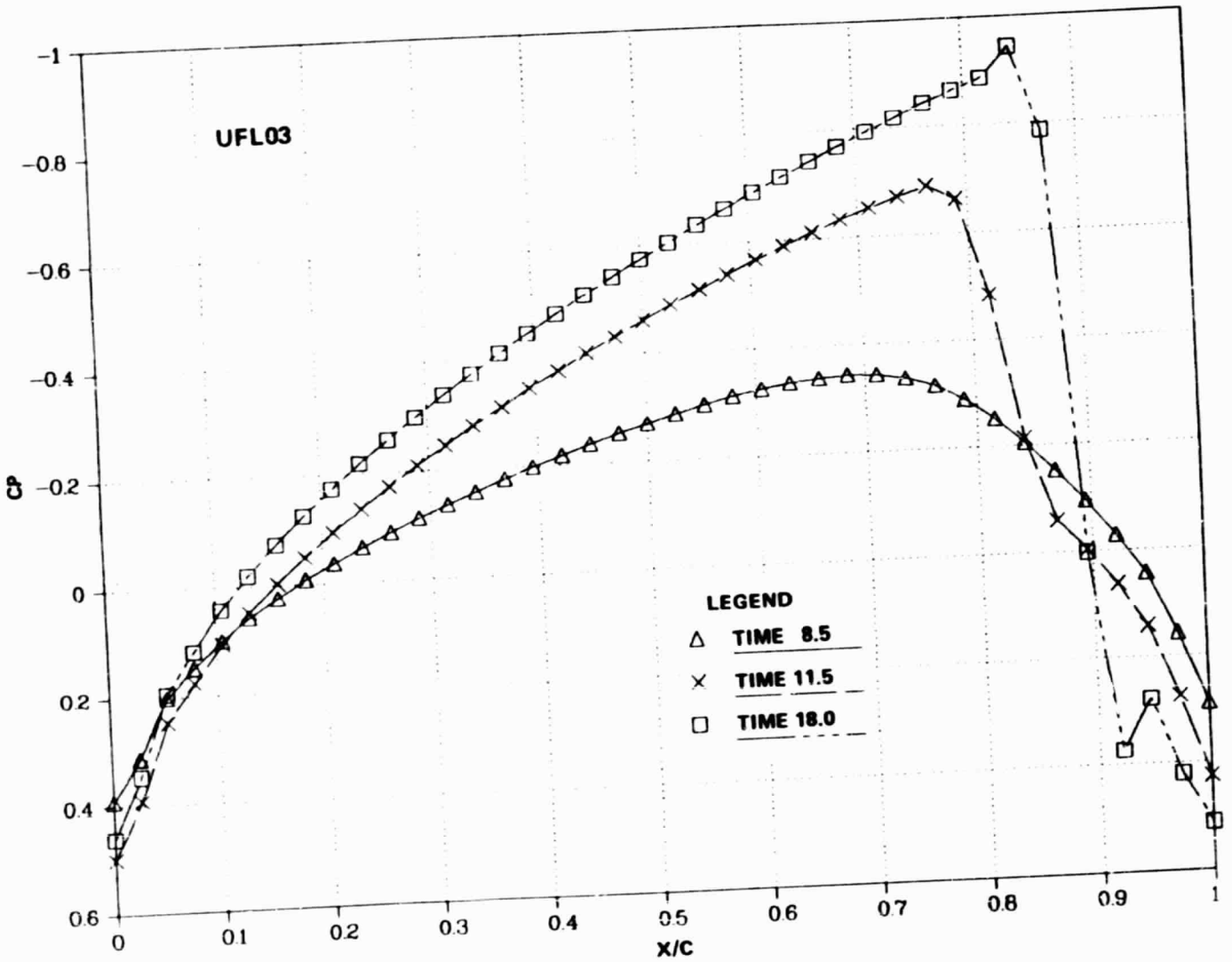

A. DURING SHOCK BUILDUP

R80-1752-004(1)W

Figure 4. — Time History of Pressures on Pulsating Airfoil — Computed by UFLO3 (Sheet 1 of 2).

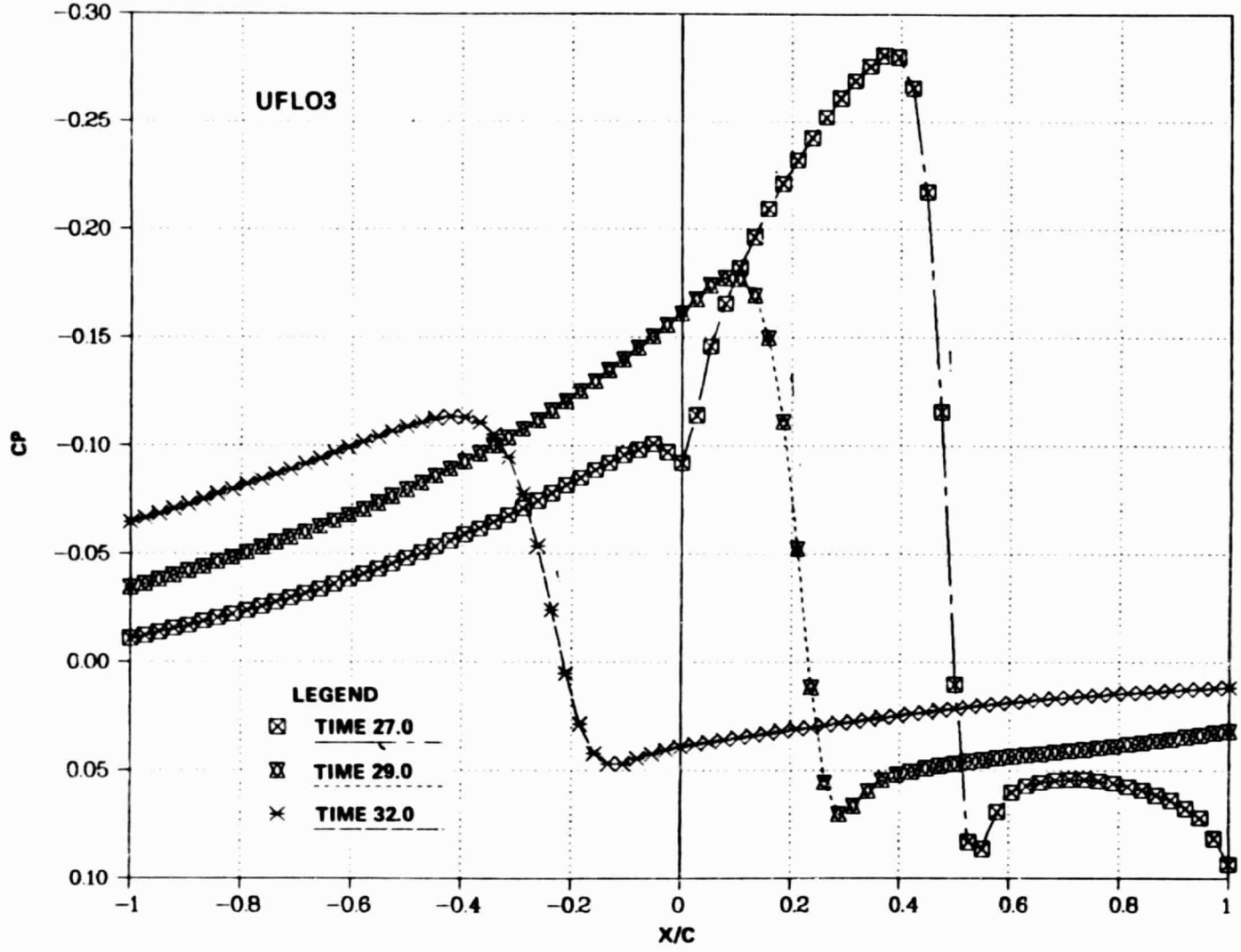

B. DURING SHOCK PROPAGATION

R80-1752-004(2)W

Figure 4. – Time History of Pressures on Pulsating Airfoil – Computed by UFLO3 (Sheet 2 of 2).

sion occurring behind the shock can be seen in Fig. 4, Sheet 1. It should be noted that a significant lag occurs between the time that the airfoil reaches maximum thickness (T = 15) and the point at which maximum shock strength is attained (T = 18.25). In the next three time slices (note that different scales are used), the shock moves rapidly forward, while diminishing in strength, and leaves the airfoil.

To determine the effect of applying the boundary conditions on the slit rather than the actual airfoil surface, results of UFLO3 and UFLO4 are compared in Fig. 5. To obtain a more dramatic difference, a 15% airfoil was used in place of the 10% airfoil previously studied; consequently, different time slices are shown. At the early time slices (Fig. 5, Sheet 1 and 2), during which the shock is formed, the results are practically identical. At later times noticeable differences occur. Comparing time T = 15 (Fig. 5, Sheet 2) with T = 25 (Fig. 5, Sheet 3) and time T = 25 with T = 30 (Fig. 5, Sheet 3), one sees that the shock speeds computed by UFLO3 during these time intervals are greater than those computed by UFLO4 (in which the boundary conditions are correctly applied on the airfoil surface). A comparison of time T = 30 with T = 35 indicates that this trend persists even after the airfoil has returned to zero thickness.

Comparison With Other Methods

Only one other operational code (Ref. 15) exists that solves the unsteady-potential-flow equations in conservation form with boundary conditions correctly applied on the instantaneous airfoil surface. (The method of Ref. 14 uses a primitive-variable formulation rather than introducing the potential function itself. Consequently, vorticity is numerically created in the flow field and degenerates the solution accuracy, particularly behind strong shocks.) Thus, comparisons between results of the present method and Ref. 15 serve as a check on the correctness of both. Furthermore, since Ref. 14 and 15 give comparisons with other, less exact formulations (Ref. 10 and 13), we will omit such investigations here.

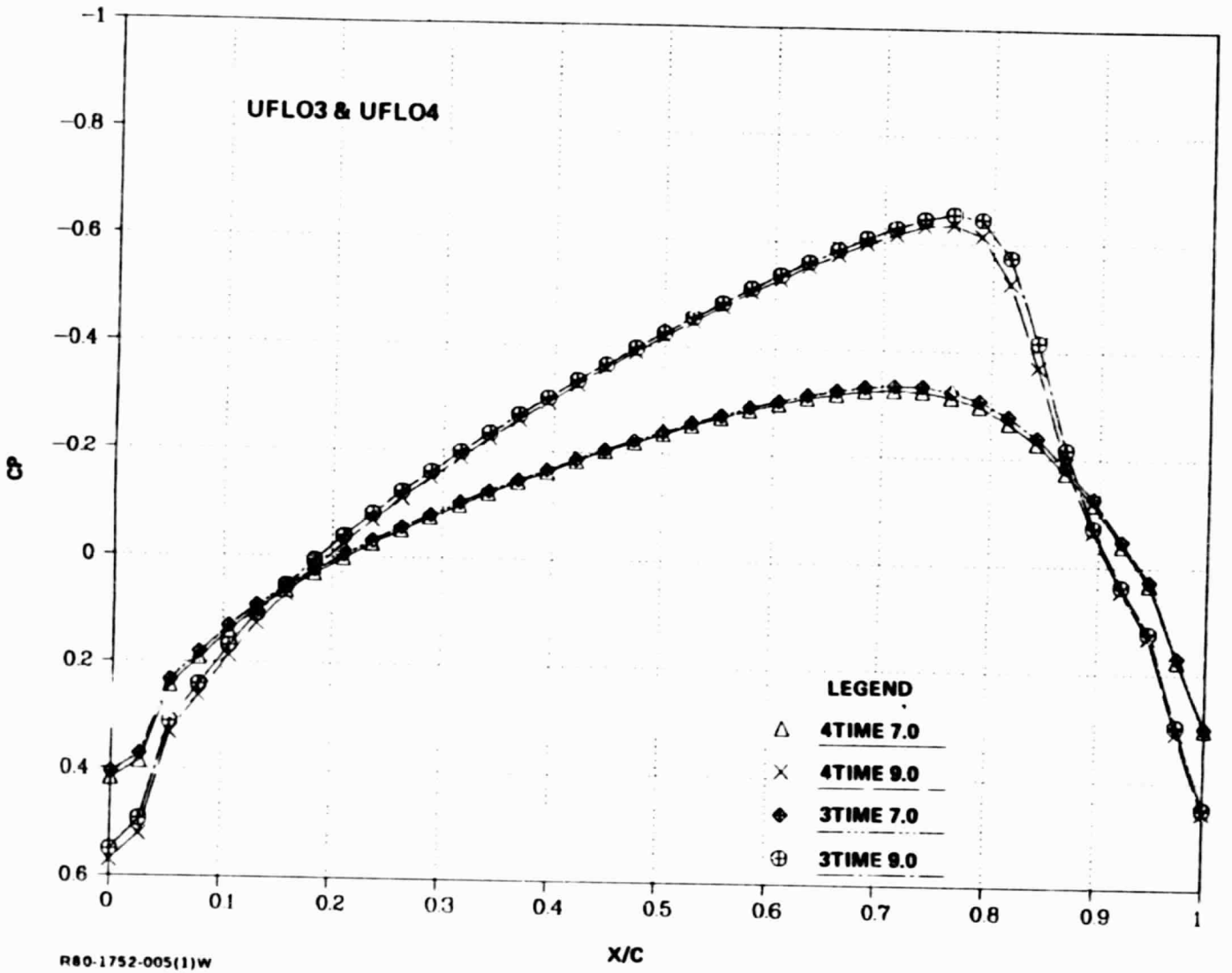

Figure 5. – Comparision of UFLO3 and UFLO4 for a 15%-Thick Airfoil, (Sheet 1 of 3).

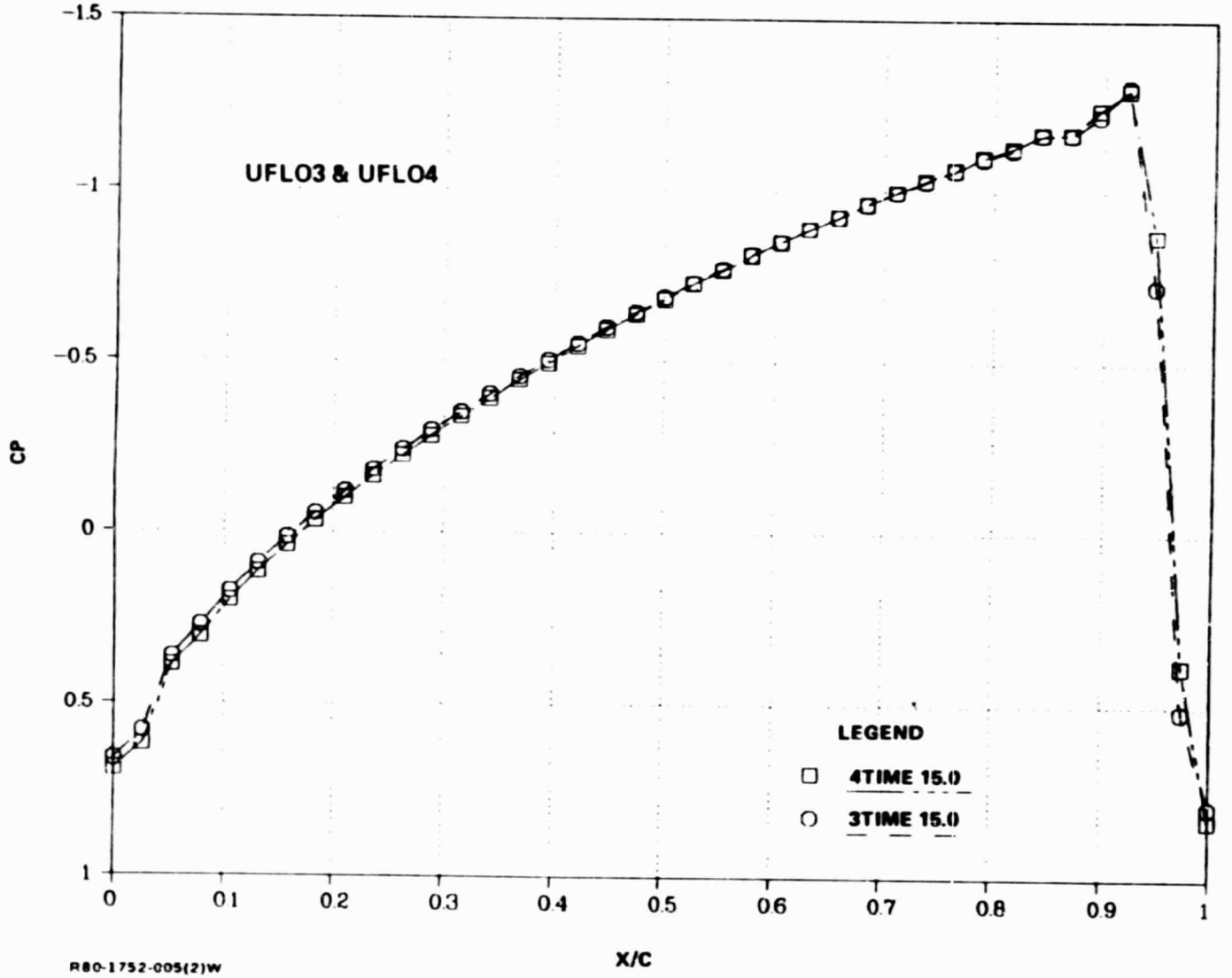

Figure 5. – Comparison of UFLO3 and UFLO4 for a 15%-Thick Airfoil, (Sheet 2 of 3).

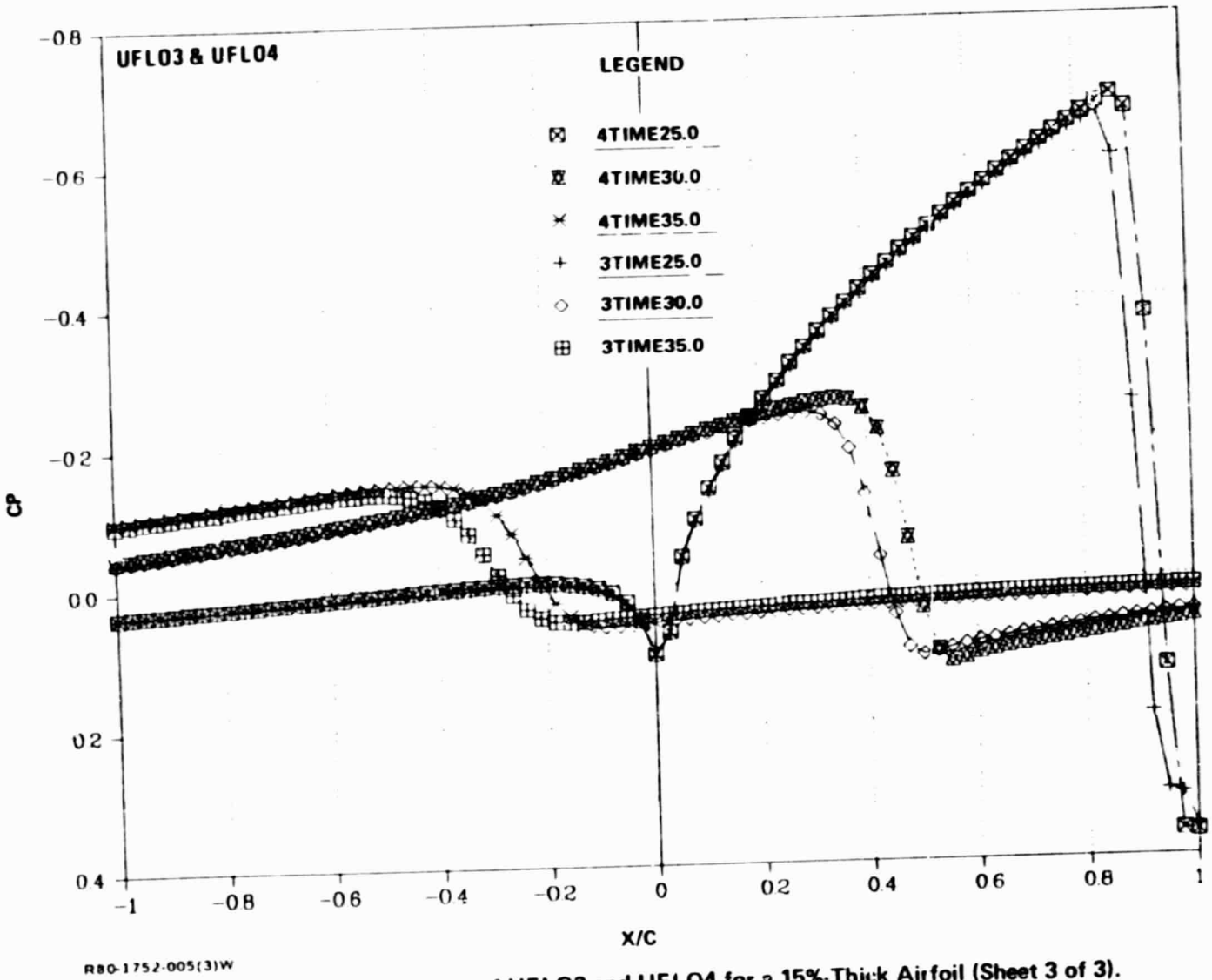

Figure 5. – Comparison of UFLO3 and UFLO4 for a 15%-Thick Airfoil (Sheet 3 of 3).

For the 10%-thick pulsating airfoil, results of UFLO4 and Goorjian's method (Ref. 15) are shown in Fig. 8. The UFLO4 results are so labeled in the plot legend; the Goorjian results are labeled "Ref. 15". As can be seen, agreement in generally good; however, there are several minor discrepancies. During shock formation, UFLO4 predicts a slightly weaker, farther aft shock. Since the shock-location difference is only one mesh width (see Fig. 6, Sheet 3), it is considered insignificant. During shock propagation, the Goorjian-method shock is smeared over larger distances and attenuates more rapidly than that of UFLO4. The better shock resolution of the present method is considered to be due to the use of artifical viscosity in lieu of artificial compressibility as used by Goorjian. Some of the remaining disparity is due to the use of slightly different grids in the two methods. Also, the calculations were performed with different time steps. The effect of this parameter in UFLO4 is discussed in a following subsection in which it is established that the time step used is adequate for accurate solutions; consequently, only small discrepancies can be attributed to this factor. In summary, the comparisons show that the present method and that of Ref. 15 give almost equivalent results for the sample problem. The only significant difference in the solutions is the degree of shock smearing and, in this aspect, the present program appears to perform somewhat better.

Stability, Accuracy, and Computing Time

To determine the effect of the time step on the stability and accuracy of the difference scheme, both UFLO3 and UFLO4 were rerun varying this parameter. The results of these investigations are summarized in Fig. 7 and 8 (UFLO3) and Fig. 9 and 10 (UFLO4), where the computed pressures are compared at two time slices. In UFLO4, the time step was successfully varied from 0.01 to 0.20 chordlenghts traveled without introducing numerical instability. Larger time steps were not attempted. In UFLO3, the time step was varied from 0.01 to 0.065. Since trends similar to those of UFLO4 were found, the larger step, 0.20, was not run. It is concluded that the algorithm has excellent stability and that the introduction of the time-varying coordinates (UFLO4) does not degrade this quality.

From inspection of Fig. 7 through 10, conclusions on the effect of time step on solution accuracy can be made. As can be seen, reasonable results were obtained for ΔT as large as 0.033. With $\Delta T = 0.065$, however, the computed shock speed during propagation is significantly less than it should be and, with $\Delta T = 0.20$, the results correlate poorly altogether with those of the other runs.

As mentioned previously, the results of Fig. 6 were obtained with $\Delta T = 0.020$. Figures 16 and 18 show that the effects of using a smaller step are quite small. Thus, the step used in the comparison studies was adequate.

Studies discussed in the next subsection indicate that a smaller amount of artificial viscosity can be successfully used. Since, for non-zero mesh widths, the artificial viscosity terms in (26) and (27) can be thought of as error terms of order ΔT, any reduction in these terms should improve accuracy for a given step size. Thus, it is likely that, by reducing the amount of artificial viscosity, accurate solutions could be obtained with a somewhat larger step size than the 0.033 discussed above.

The computational time required for the algorithm is roughly 7.0×10^{-5} seconds per time step per grid point on the CDC 7600 computer. For the sample problem with $\Delta T = 0.033$, the time required for a time history of 32 chordlengths traveled is about 6 minutes.

Effect of Artificial Viscosity

To determine the amount of artificial viscosity necessary to sharply resolve shocks, variations of the parameter ε were made in the sample problem. The results of this investigation are shown in Fig. 11 for a single point in the time history. It can be seen from this figure that the value 0.15 used in all previous calculations can be varied by approximately 20% without introducing excessive overshoots or smearing near the shock. As expected, variations of ε have no effect away from the shock.

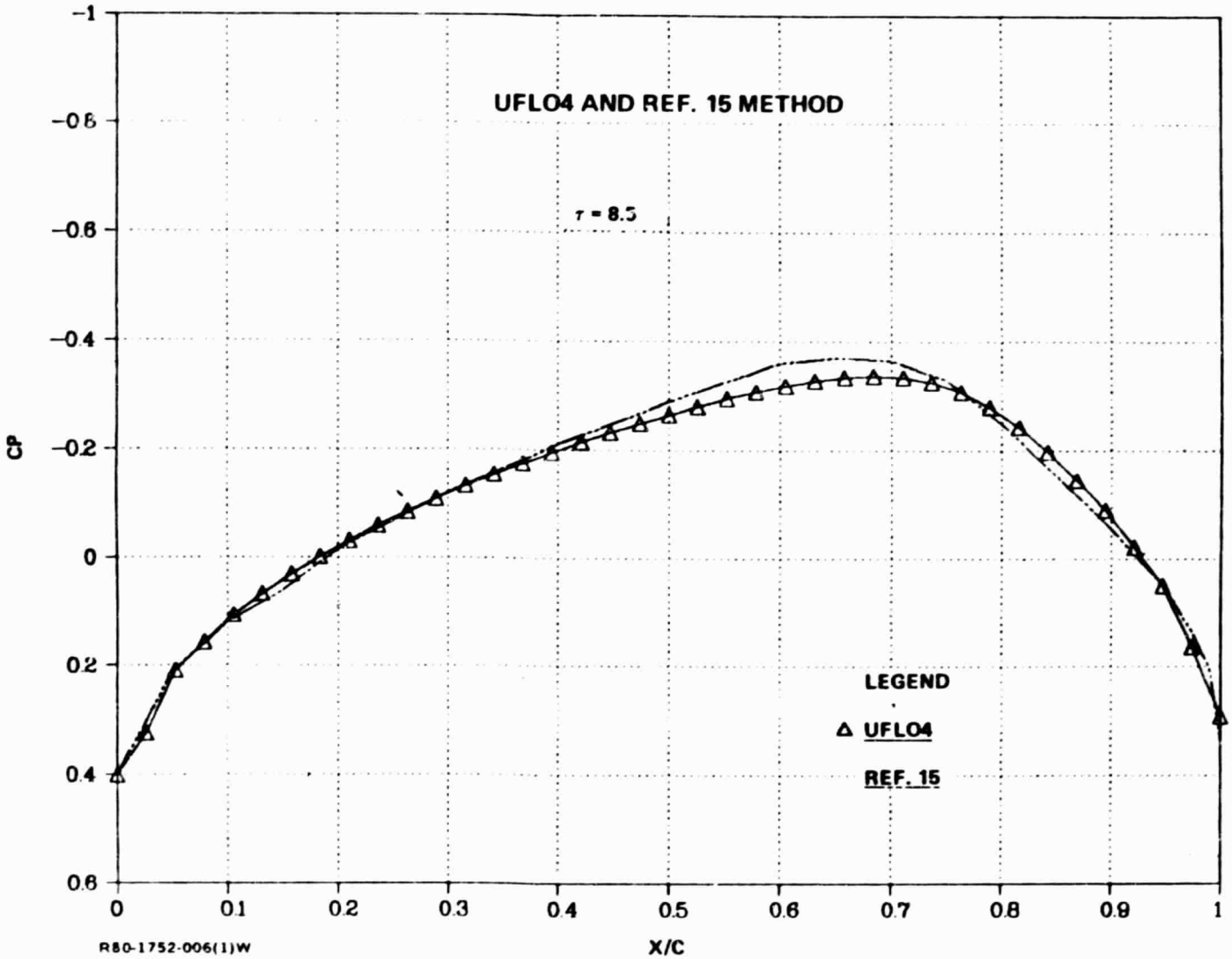

Figure 6. – Comparison of UFLO4 with Goorjian Program (Sheet 1 of 6).

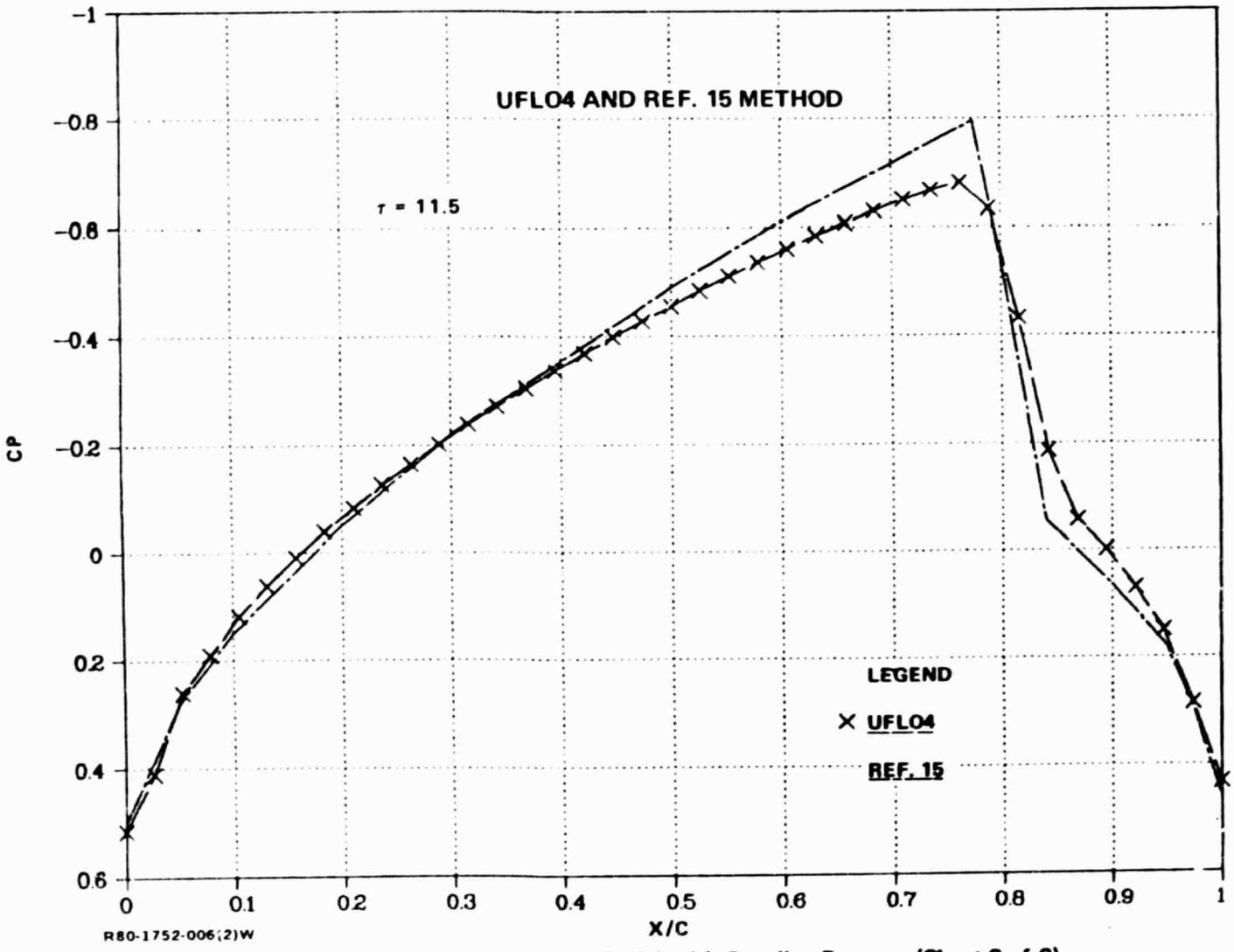

Figure 6. – Comparison of UFLO4 with Goorjian Program (Sheet 2 of 6).

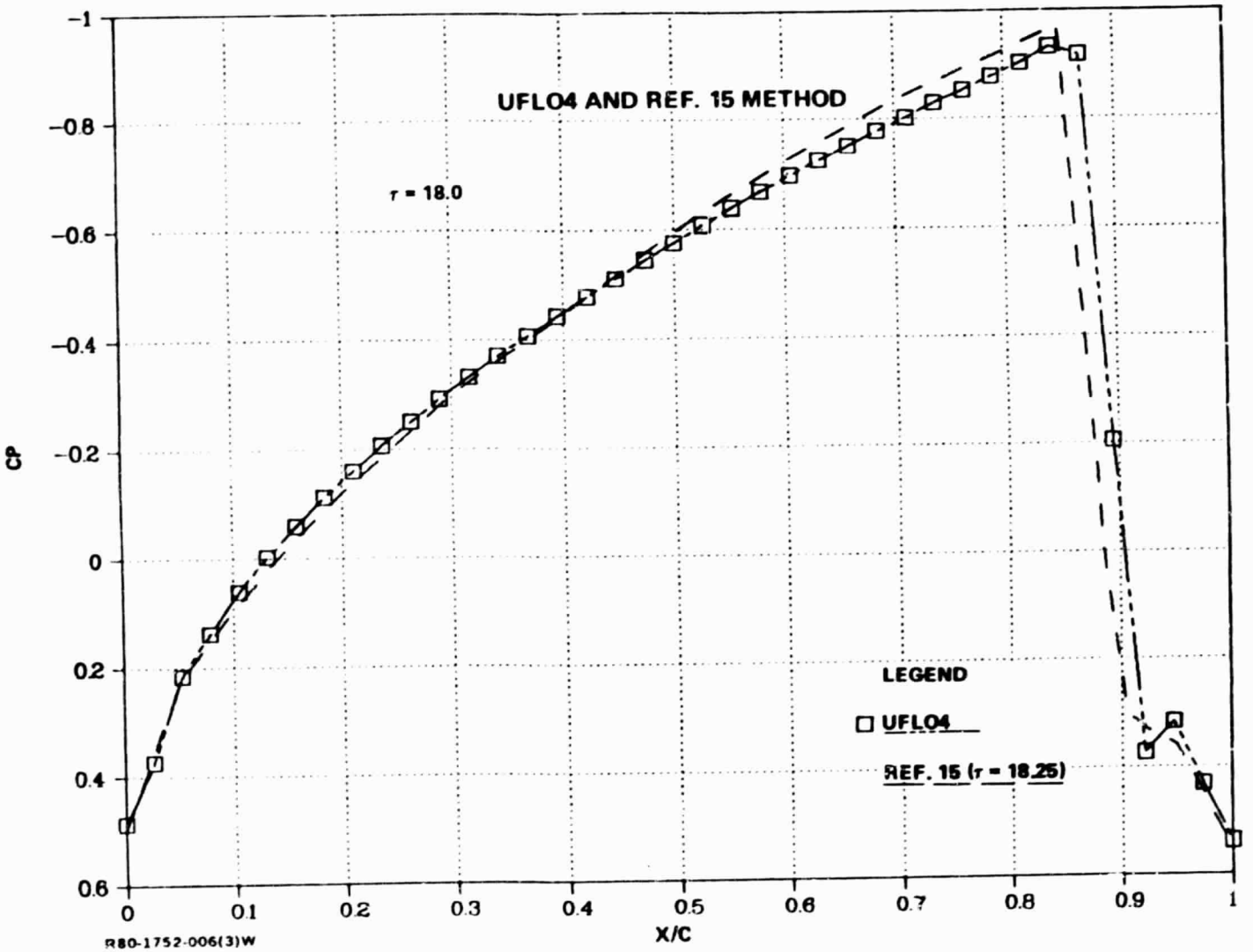

Figure 6. – Comparison of UFLO4 with Goorjian Program (Sheet 3 of 6).

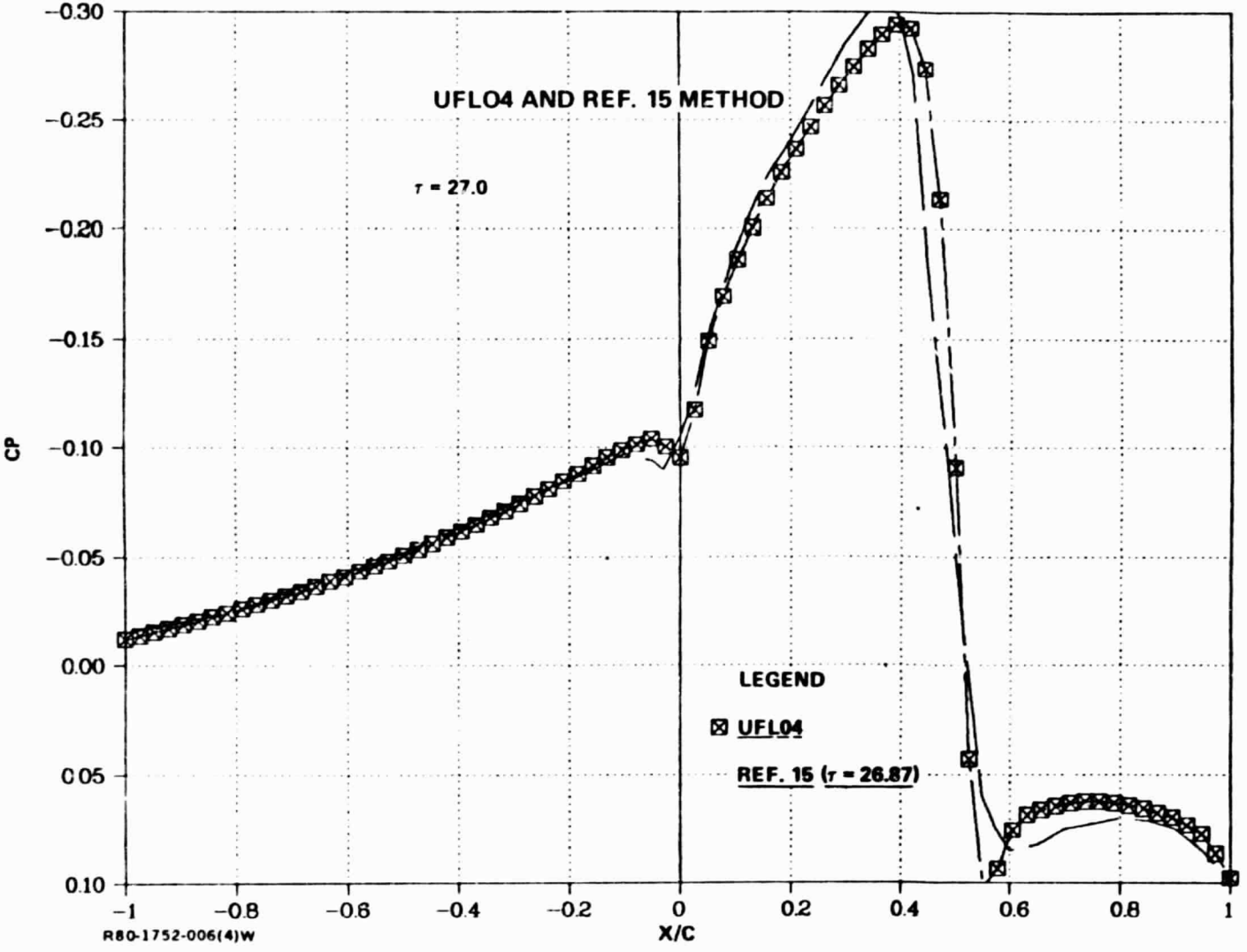

Figure 6. – Comparison of UFLO4 with Goorijan Program (Sheet 4 of 6).

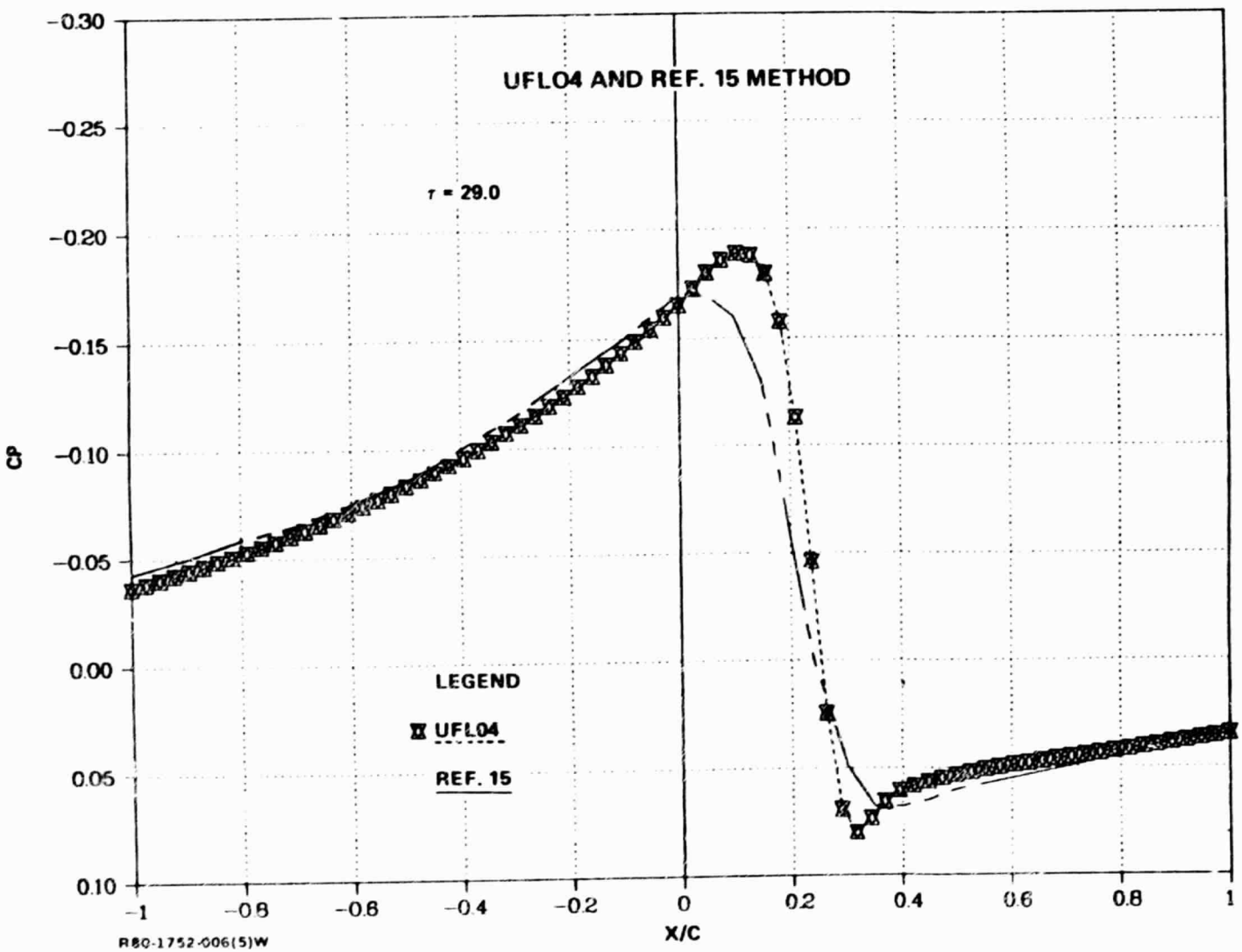

Figure 6. – Comparison of UFLO4 with Goorijan Program (Sheet 5 of 6)..

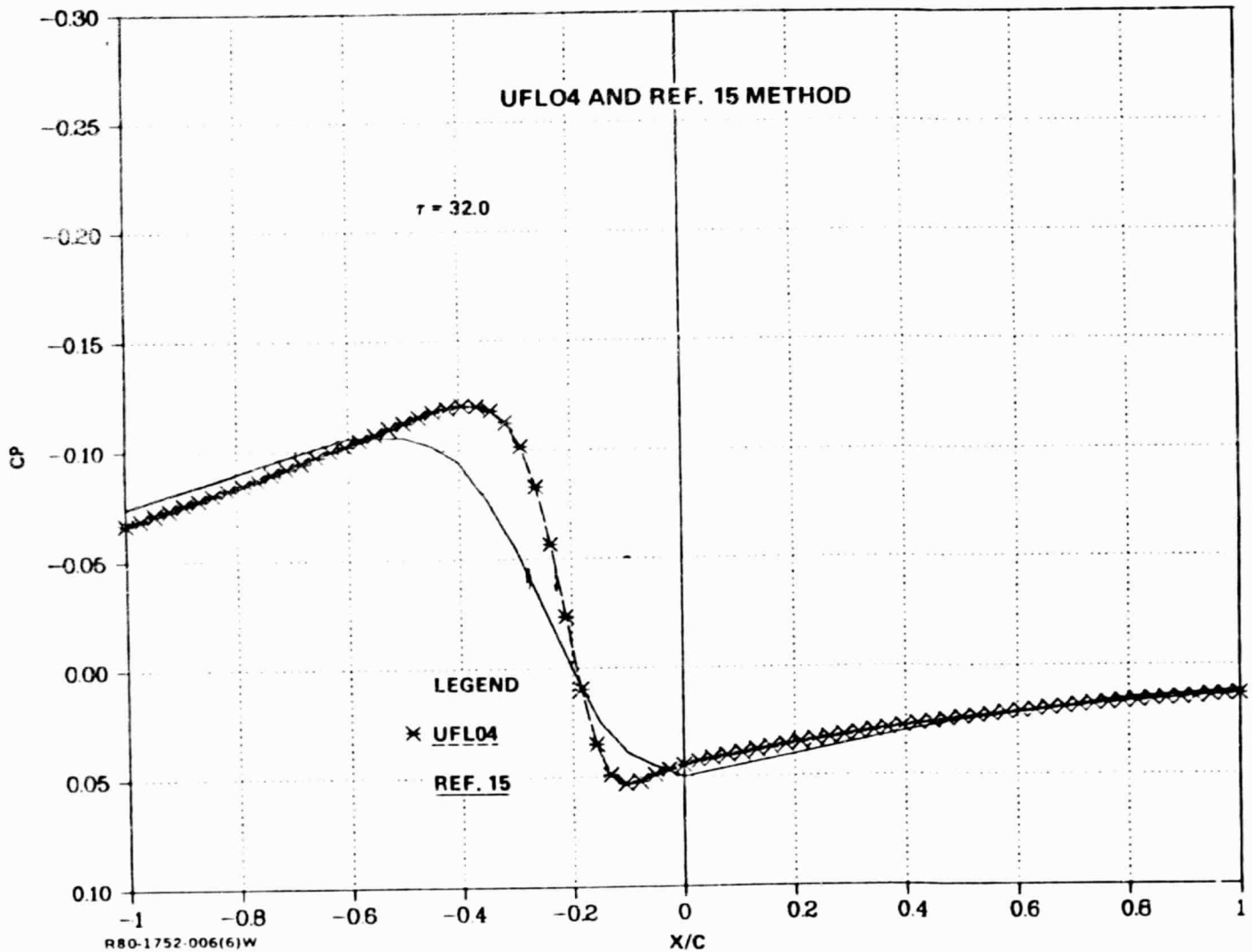

Figure 6. — Comparison of UFLO4 with Goorjian Program (sheet 6 of 6).

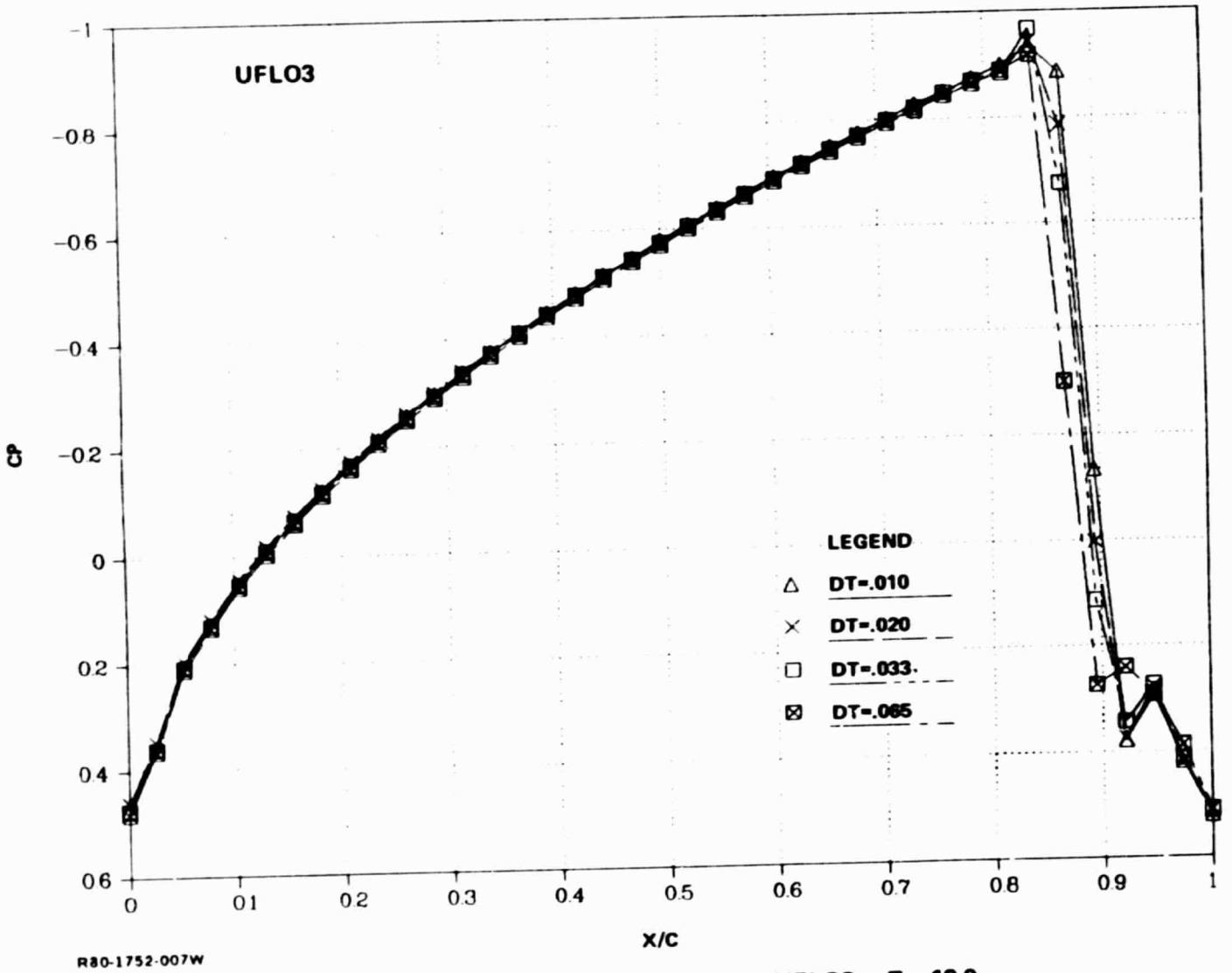

Figure 7. — Effect of Integration Step: UFLO3 at T = 18.0

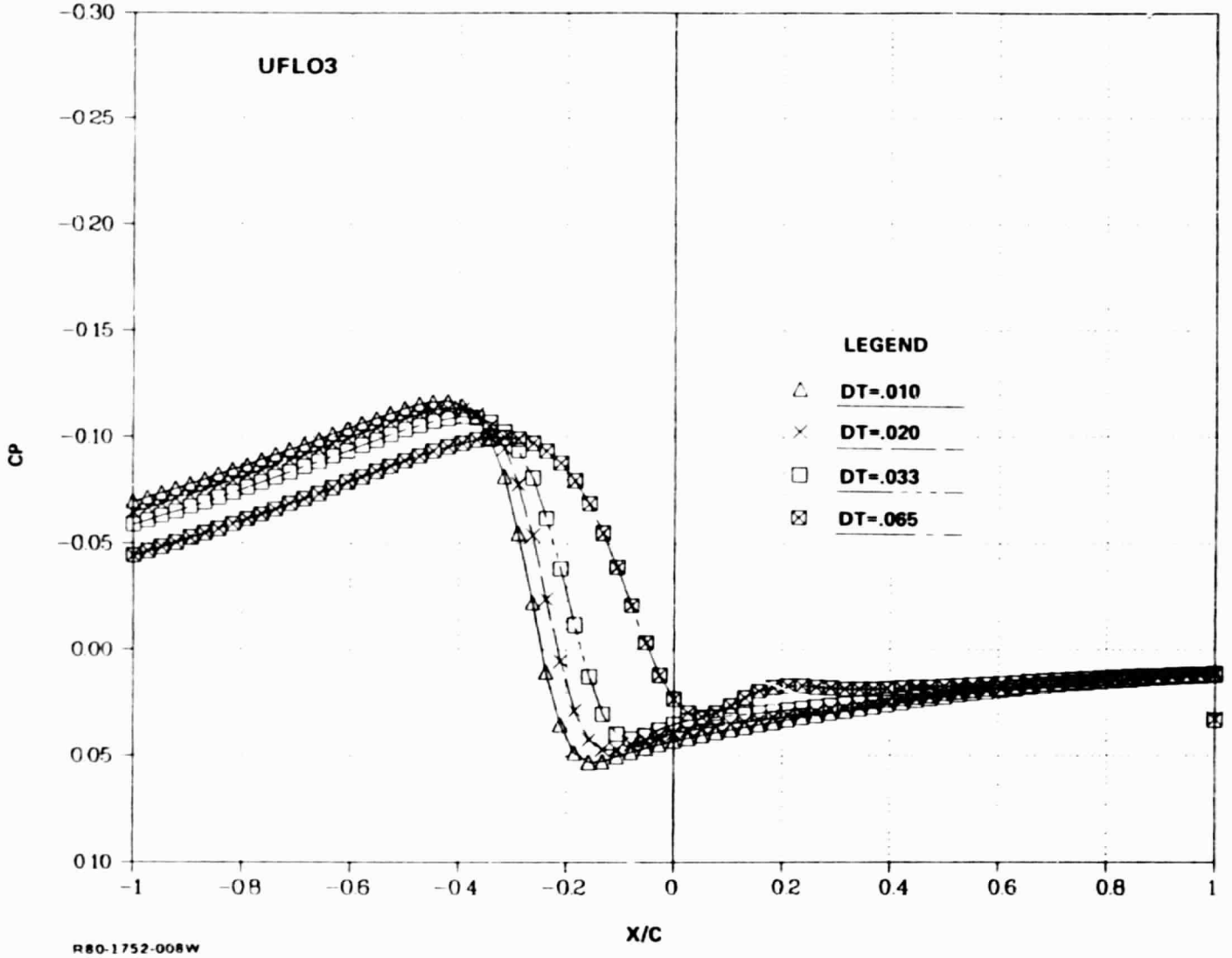

Figure 8. – Effect of Integration Step: UFLO3 at T = 32.0.

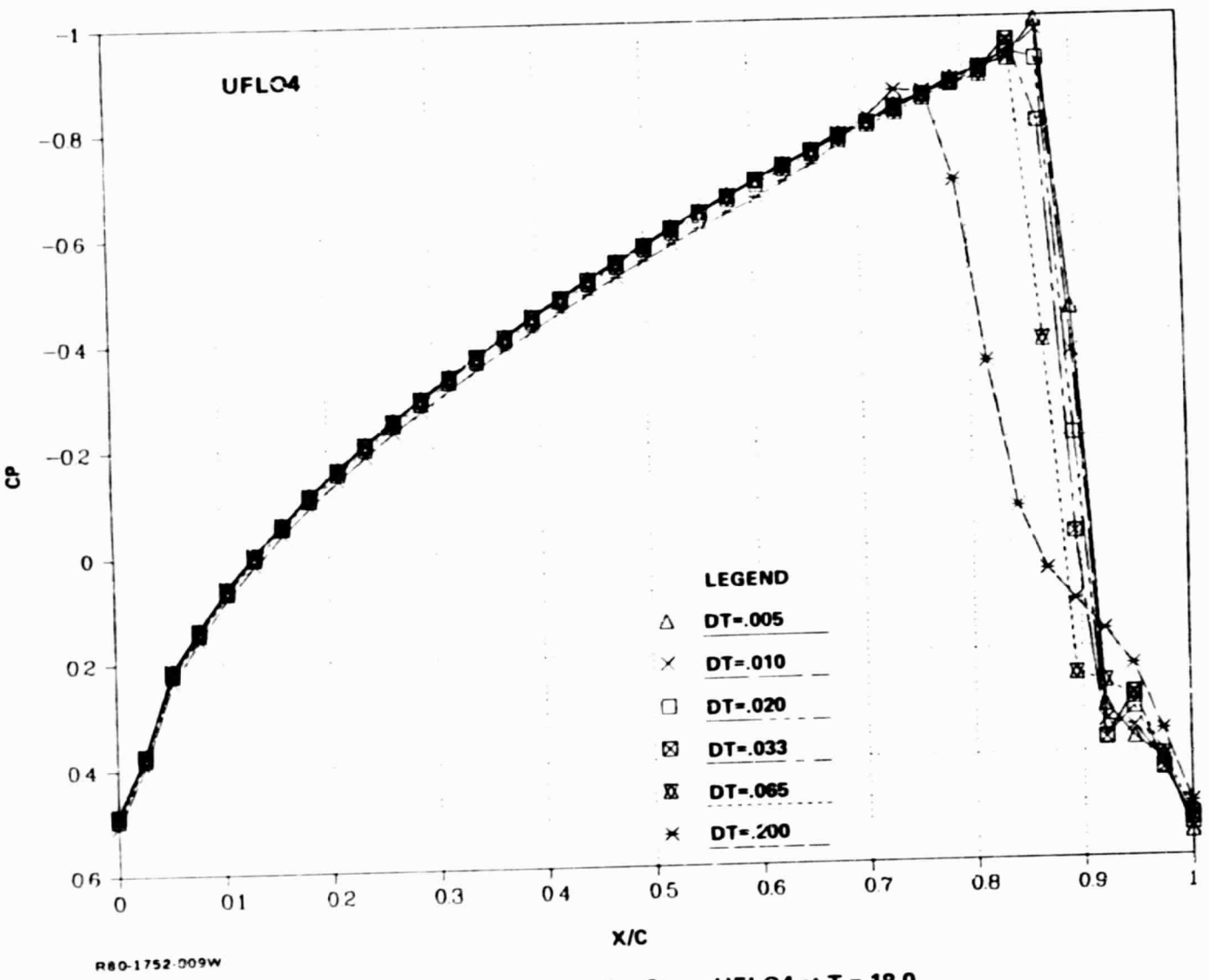

Figure 9. — Effect of Integration Step: UFLO4 at T = 18.0.

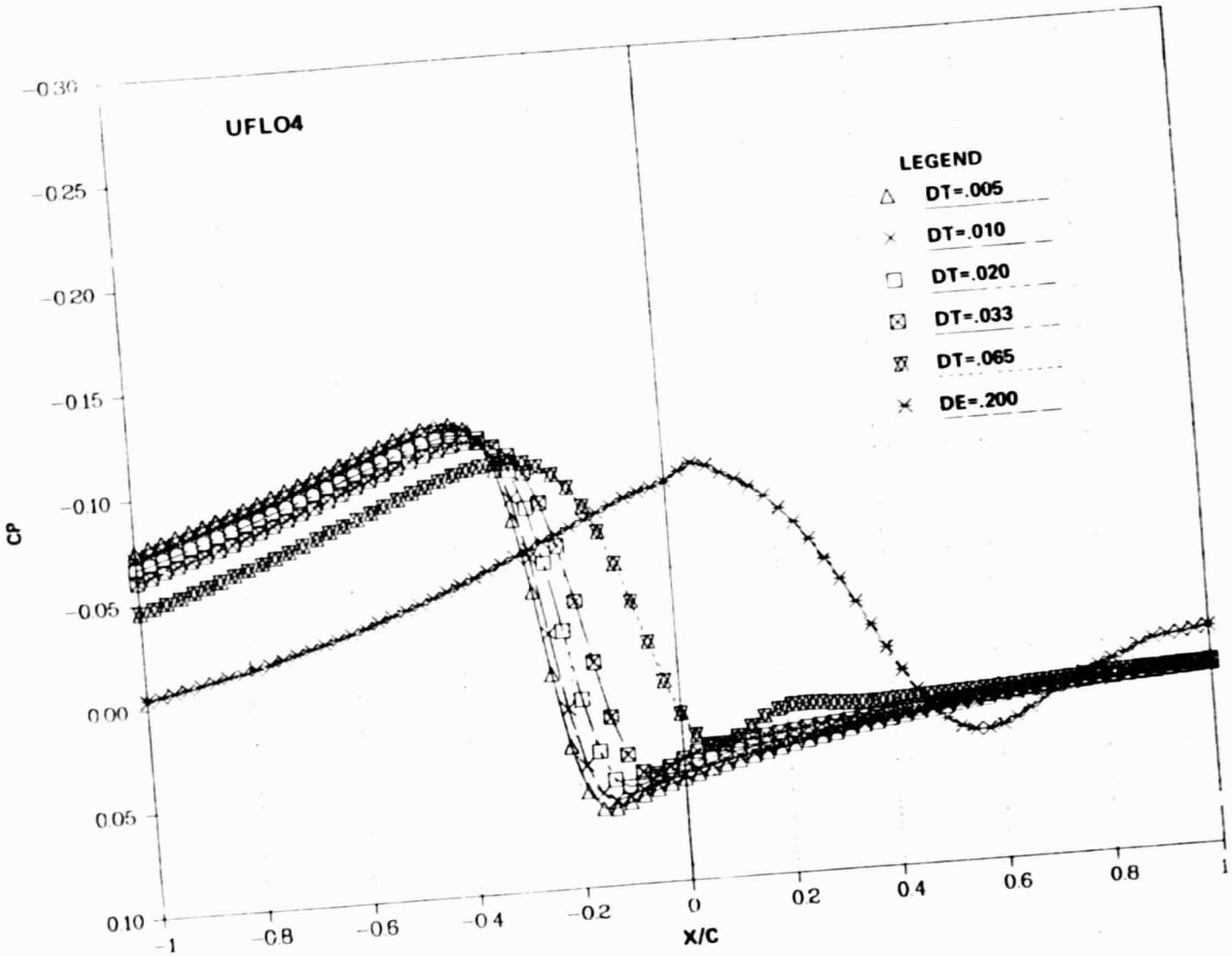

R80-1752-010W

Figure 10. — Effect of Integration Step: UFLO4 at T = 32.0

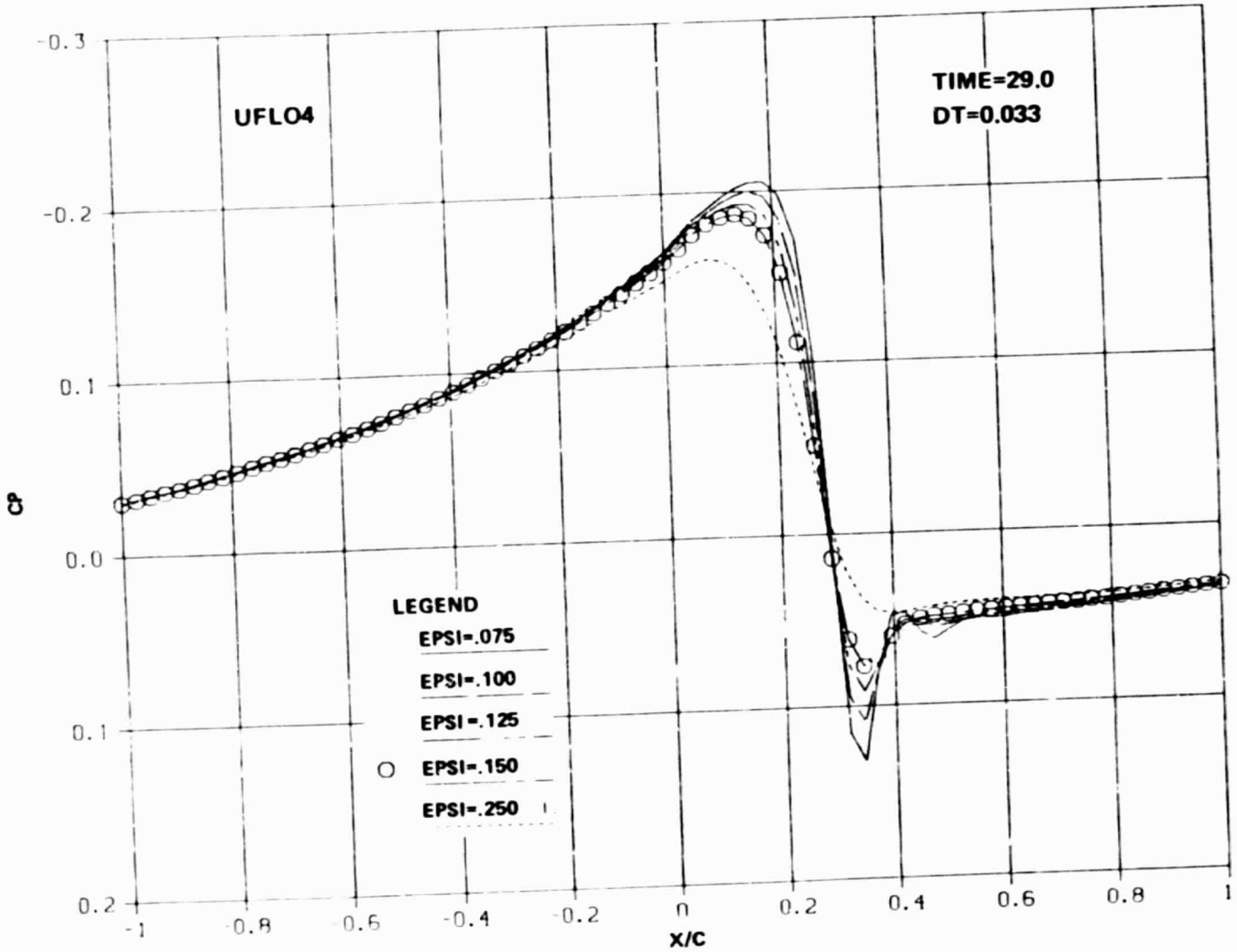

R80-1752-011W

Figure 11. – Effect of Variation of the Artificial Viscosity Coefficient ϵ.

6 - CONCLUSIONS AND RECOMMENDATIONS

An accurate algorithm with excellent numerical stability has been developed for the two-dimensional unsteady full-potential equation in conservation form, using time-varying sheared-rectilinear, body-conforming coordinates. The method has been demonstrated on the highly nonlinear transonic flow arising from an airfoil with pulsating thickness. The results of this demonstration have been verified by comparison with those reported in Ref. 15.

Two recommendations are made to increase the accuracy and efficiency of the procedure. The first is to introduce switched artificial viscosity as discussed in the THEORY section. This change would localize the artificial-viscosity terms to regions where they are needed, thereby improving the accuracy for a given time step. Consequently, larger time steps could be used with a resultant decrease in computing time. The second suggestion is to modify the manner in which the operators $D_\xi \rho D_\xi$ and $D_\eta \bar{\rho} D_\eta$ in (26) and (27) are evaluated. A three-point scheme could be constructed in place of a five-point scheme. To accomplish this, densities midway between mesh points would be evaluated by averaging the values from the two adjacent nodes. This modification would result in reducing the system in (31) from block-five-diagonal to block-three-diagonal. It can be shown that the computing time required to solve the smaller-bandwidth system is roughly half that required for the larger system.

To enable the method to handle realistic blunt-nosed airfoils, it is further recommended that the code be modified to use a curvilinear coordinate transformation. In particular, a parabolic (C-mesh) transformation is suggested. Additional efforts should then be focused on extensions to the case of a lifting airfoil and improved treatment of the far-field boundary conditions.

7 - REFERENCES

1. Ehlers, F. E., "A Finite Difference Method for the Solution of the Transonic Flow Around Harmonically Oscillating Wings," NASA CR-2257, July 1974.

2. Traci, R. M., Albano, E. D., and Farr, J. L., "Perturbation Method for Transonic Flows About Oscillating Airfoils," AIAA Journal, Vol. 14, No. 9, September 1976.

3. Cunningham, A. M., "An Oscillatory Kernel Function Method for Lifting Surfaces in Mixed Transonic Flow," AIAA Paper No. 74-359, 1974.

4. Liu, D. D., "A Lifting Surface Theory Based on an Unsteady Linearized Transonic Flow Model," AIAA Paper No. 78-501, 1978.

5. Fung, F. Y., Yu, N. J., and Seebass, R., "Small Unsteady Perturbations in Transonic Flows," AIAA Paper No. 77-675, 1977.

6. Tijdeman, H., "Investigations of the Transonic Flow Around Oscillating Airfoils," NLR Report TR 77090 U, 1978.

7. Magnus, R. J., and Yoshihara, H., "Unsteady Transonic Flow Over an Airfoil," AIAA Journal, Vol. 14, No. 12, December 1975.

8. Lerat, A., and Sides, J., "Calcul Numerique D'ecoulements Transsoniques Instationnaires," ONERA TP No. 1977-19E.

9. Beam, R. M., and Warming, R. F., "Numerical Calculations of Two-Dimensional Unsteady Transonic Flows with Circulation," NASA TN D-7605, 1974.

10. Ballhaus, W. F., and Steger, J. L., "Implicit Approximate-Factorization Schemes for the Low-Frequency Transonic Equation," NASA TM X-73,082, November 1975.

11. Ballhaus, W. F., and Goorjian, P. M., "Implicit Finite Difference Computations of Unsteady Transonic Flows about Airfoils," AIAA Journal, Vol. 15, No. 12, December, 1977.

12. Ballhaus, W. F., and Goorjian, P. M., "Computation of Unsteady Transonic Flows by the Indicial Method," AIAA Journal, Vol. 16, No. 2, February 1978.

13. Isogai, K., "Calculation of Unsteady Transonic Flow Over Oscillating Airfoil Using the Full Potential Equation," AIAA Paper No. 77-448, 1977.

14. Chipman, R., and Jameson, A., "Fully Conservative Numerical Solutions for Unsteady Irrotational Transonic Flow about Airfoils," AIAA Paper No. 79-1555, presented at 12th Fluid and Plasma Dynamics Conference, July 1979.

15. Goorjian, P. M., "Computations of Unsteady Transonic Flow Governed by the Conservative Full Potential Equation Using an Alternating Direction Implicit Algorithm," NASA CR-152274, June 1979.

16. Sankar, N. L., and Tassa, Y., "An Algorithm for Unsteady Transonic Potential Flow Past Airfoils," paper presented at the Seventh International Conference on Numerical Methods in Fluid Dynamics, June, 1980.

17. Isaacson, E., and Keller, H. B., Analysis of Numerical Methods, Wiley and Sons, Inc., New York, 1966.

18. Jameson, A., "Transonic Flow Calculations," Notes of Lecture presented at the Von Karman Institute, Belgium, March 1976.

APPENDIX A - MAPPED COORDINATES

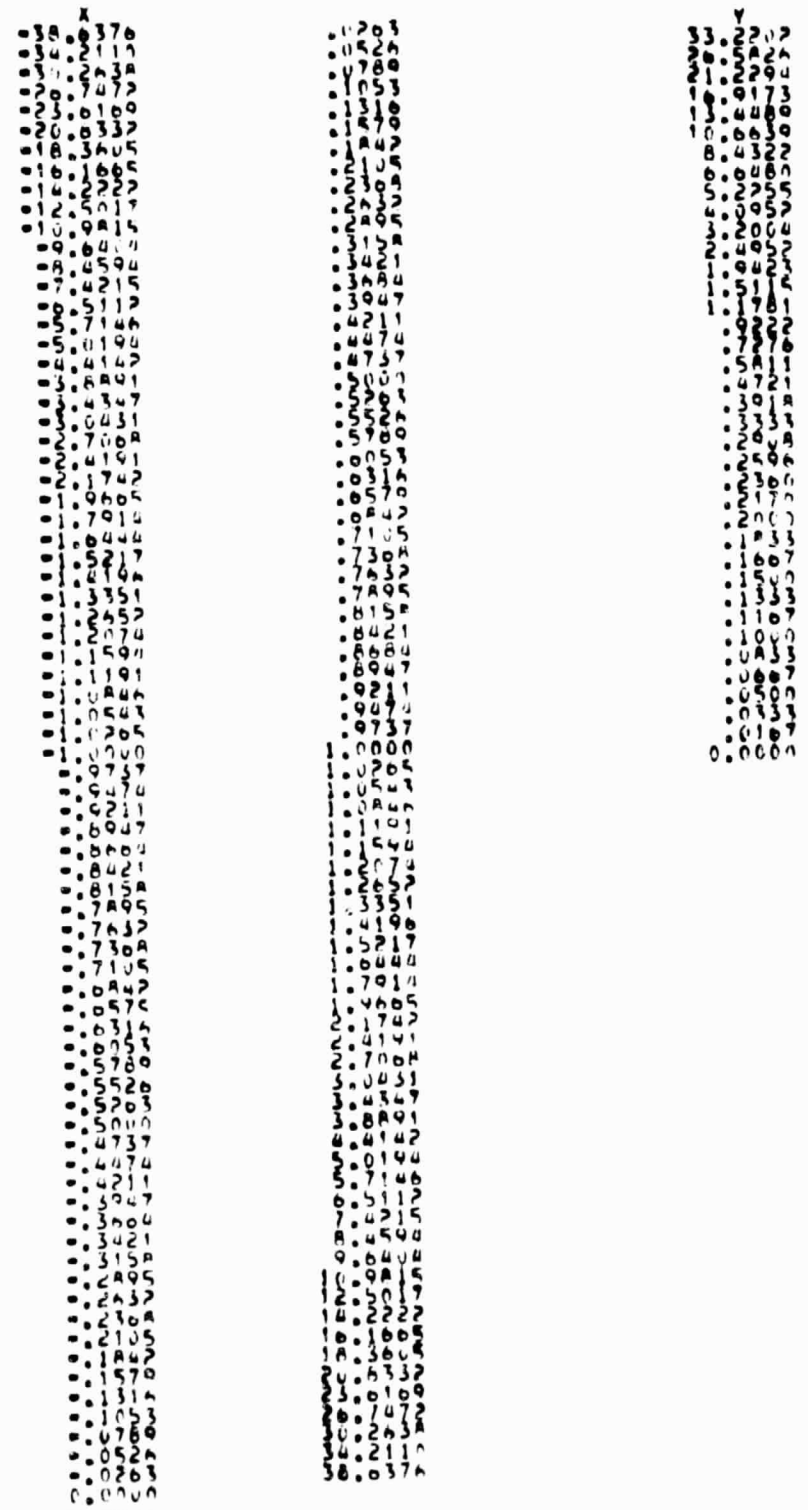

RB0-1752-012W